Published by CERN in the Proceedings of the 2013 European School of High-Energy Physics, Parádfürdő, Hungary, 5 – 18 June 2013, edited by M. Mulders and G. Perez, CERN–2015–004 (CERN, Geneva, 2015)

Higgs Physics

J. Ellis
Department of Physics, King's College London, London WC2R 2LS, United Kingdom;
Theory Division, CERN, CH-1211 Geneva 23, Switzerland

Abstract
These lectures review the background to Higgs physics, its current status following the discovery of a/the Higgs boson at the LHC, models of Higgs physics beyond the Standard Model and prospects for Higgs studies in future runs of the LHC and at possible future colliders.

KCL-PH-TH/2013-49, LCTS/2013-36, CERN-PH-TH/2013-315

1 Motivations and Context

1.1 To Higgs or not to Higgs?

The Standard Model describes all the visible matter in the Universe in terms of a limited number of fermionic constituents of matter: six quarks, three charged leptons and three light neutrinos. It also comprises three fundamental gauge interactions between these constituents, namely the electromagnetic, strong and weak forces, to which should be added gravitation. The Standard Model is in good agreement with all confirmed experimental results from particle accelerators. However, there was, until July 4th 2012, one crucial missing ingredient: the origin of particle masses. Without a mass for the electron there would be no atoms, as electrons would escape from nuclei at the speed of light, and the weak interactions would not live up to their name: they would be stronger than electromagnetism. So discovering the origin of particle masses has been a Big Deal.

In addition to elucidating the origin of particle masses and establishing whether a/the Higgs boson exists, there are many important open questions beyond the Standard Model. Why are there so many different types of matter particles? Why do weak interactions mix them the way they do? How/why do they discriminate between matter and antimatter, and might this difference explain the dominance of matter over antimatter in the Universe today? What is the nature of the invisible dark matter that, according to astrophysicists and cosmologists, dominates over the visible matter described by the Standard Model? Are the fundamental forces unified, and what is the full quantum theory of gravity?

The key to answering many of these other questions may be provided by finding the origin of particle masses. For example, decays of the Higgs boson may discriminate between matter and antimatter, and might lie at the origin of the cosmological matter-antimatter asymmetry. In many theoretical extensions of the Standard Model, the Higgs boson is accompanied by other new particles, the lightest of which might provide the astrophysical dark matter. A possible unified theory of all the elementary particle interactions might employ a symmetry-breaking mechanism analogous to that in the Standard Model, and the existence of any light 'elementary' scalar boson would pose a challenge for many quantum theories of gravity.

The equations describing the gauge interactions of the Standard Model do not discriminate between matter particles with the same quantum numbers, which differ only in their masses. The mass-generation mechanism must discriminate between these otherwise-identical particles of matter and between the different force-carrying vector bosons: it must break the symmetries between them. One way to achieve this might be to break the symmetry explicitly in the equations, but then the calculability of the theory would be lost. The alternative is to retain symmetric equations but break the symmetry in their solutions.

http://dx.doi.org/10.5170/CERN-2015-004.117

The issue then is whether to break the symmetry throughout space, or via boundary conditions. The latter is not possible in conventional three-dimensional space, since it has no boundaries. However, it would be possible in theories with additional dimensions of space: one could postulate different behaviours in the extra dimension(s) for different particle species. The discovery of a/the Higgs boson at the LHC [1, 2] has somewhat deflated interest in extra-dimensional models, unless their spectrum features a low-mass excitation that resembles closely the Higgs boson of the Standard Model.

This discovery seems to mark the latest success of a long-running theoretical strategy in particle physics: when in trouble, postulate one of more new particles. A partial list includes reconciling quantum mechanics and special relativity (antimatter), nuclear spectra (the neutron), the continuous spectrum in β decay (the neutrino), nucleon-nucleon interactions (the pion), the suppression of $\mu \to e\gamma$ (the second neutrino), flavour SU(3) (Ω^- and quarks), the suppression of flavour-changing neutral currents (charm), CP violation (the third generation), strong dynamics (the gluons), the discovery of the τ lepton (the b and t quarks), weak interactions (the $W^\pm$ and Z^0), and their renormalizability (a/the Higgs boson) [1].

The discovery of a/the Higgs boson marks the completion of the Holy Trinity of particle types seen in Table 1.2. It has been known for decades that the only type of field theory capable of making non-trivial over many magnitudes of energy is a renormalizable one. Also, it has been a theorem for some 40 years that such a theory could only contain (i) gauge vector bosons, (ii) spin-1/2 fermions, and (iii) scalar bosons. Specification of a renormalizable theory is completed by choosing (a) the gauge group, (b) the fermion representations, and (c) the scalar fields used to realize the desired symmetry-breaking pattern. We have long known that the answer (so far) to (a) is SU(3)×SU(2)×U(1) and that the fermion representations are triplets of SU(3) and singlets and doublets of SU(2). Finally we have an example of category (iii), a scalar boson, and there is strong evidence that it is responsible for (c) electroweak symmetry breaking.

The first of these lectures describes the long road towards the discovery of a/the Higgs boson, the second lecture describes the state of our knowledge after Run 1 of the LHC, and the third lecture outlines some of the prospects for future studies, including supersymmetric Higgs bosons and concepts for Higgs factories.

1.2 Summary of the Standard Model

Table 1.2 summarizes the particle content of the Standard Model [3–6]. The electromagnetic and weak interactions are described by an $SU(2)_L \times U(1)_Y$ group [7], where the subscript L reminds us that the weak SU(2) group acts only the left-handed fermions, and Y is the hypercharge. The $SU(2)_L \times U(1)_Y$ part of the Standard Model Lagrangian may be written as

$$\begin{aligned} \mathcal{L} &= -\frac{1}{4}\mathbf{F}^a_{\mu\nu}\mathbf{F}^{a\mu\nu} \\ &+ i\bar{\psi}\not{D}\psi + h.c. \\ &+ \psi_i y_{ij} \psi_j \phi + h.c. \\ &+ |D_\mu \phi|^2 - V(\phi) \ , \end{aligned} \tag{1}$$

which is short enough to write on a T-shirt!

The first two lines of (1) have been confirmed in many different experiments with a high degree of accuracy. However, consistency with the precision electroweak measurements made at LEP and other accelerators agreed with the Standard Model if only if there was a relatively light Higgs boson weighing < 180 GeV or so [8, 9]. However, until July 2012 there was no direct experimental evidence for the last two lines [1, 2]. One of the main objectives of the LHC was to discover whether they are right, need

[1] Outstanding examples include dark matter (the axion or a WIMP?) and the fine-tuning problem (supersymmetry?). Depressed advocates of supersymmetry should remember that it took 48 years to discover a/the Higgs boson, whereas at the time of writing four-dimensional supersymmetric gauge theories are 'only' 40 years old.

Gauge bosons	Scalar bosons
γ, W^+, W^-, Z^0, $g_{1...8}$	ϕ (Higgs)

Spin-1/2 Fermions

Quarks (each with 3 colour charges)	Leptons
Charges $+2/3$: $\begin{pmatrix} u \\ d \end{pmatrix}, \begin{pmatrix} c \\ s \end{pmatrix}, \begin{pmatrix} t \\ b \end{pmatrix}$	Charges 0 : $\begin{pmatrix} \nu_e \\ e^- \end{pmatrix}, \begin{pmatrix} \nu_\mu \\ \mu^- \end{pmatrix}, \begin{pmatrix} \nu_\tau \\ \tau^- \end{pmatrix}$
$-1/3$:	-1 :

Table 1: The particle content of the Standard Model with a minimal Higgs sector

modification, or are simply wrong. The most important result of the first run of the LHC has been to find some evidence that these lines do indeed contain a grain of truth.

The first line in (1) is the kinetic term for the gauge sector of the electroweak theory, with a running over the total number of gauge fields: three associated with SU(2)$_L$, which we call B^1_μ, B^2_μ, B^3_μ, and one associated with U(1)$_Y$, which we call A_μ. Their field-strength tensors are

$$F^a_{\mu\nu} = \partial_\nu B^a_\mu - \partial_\mu B^a_\nu + g\varepsilon_{bca} B^b_\mu B^c_\nu \text{ for a} = 1, 2, 3 \, ; \tag{2}$$

$$f_{\mu\nu} = \partial_\nu A_\mu - \partial_\mu A_\nu \, . \tag{3}$$

In (2), g is the coupling constant of the weak-isospin group SU(2)$_L$, and the ε_{bca} are its structure constants. The last term in this equation stems from the non-Abelian nature of SU(2). The gauge fields are massless in the absence of any scalar fields, but we will see later how specific linear combinations of the four electroweak gauge fields can acquire masses by spontaneous symmetry breaking induced by a scalar field.

The second line in Eq. (1) describes the interactions between the matter fields ψ, described by Dirac equations, and the gauge fields via covariant derivatives.

The third line is the Yukawa sector and incorporates the interactions between the matter fields and the scalar field ϕ that is responsible for giving fermions their masses when electroweak symmetry breaking occurs.

The fourth and final line is the engine room of the scalar sector. The first piece is the kinetic term for ϕ with the covariant derivative defined here to be

$$D_\mu = \partial_\mu + \frac{ig'}{2} A_\mu Y + \frac{ig}{2} \tau \cdot \mathbf{B}_\mu \, , \tag{4}$$

where g' is the U(1) coupling constant, and Y and $\tau \equiv (\tau_1, \tau_2, \tau_3)$ are the Pauli matrices that generate, respectively, U(1) and SU(2). The second piece of the final line of (1) is the effective potential $V(\phi)$ constructed in such a way that its minimization gives rise to a non-zero v.e.v. for the scalar field, and hence spontaneous electroweak symmetry breaking.

1.3 The (NG)AEBHGHKMP Mechanism

This mechanism is often called the Higgs mechanism, but the history is quite complicated, with many antecedents to the Higgs papers, with antecedents in condensed-matter physics, e.g., in the theories of superfluidity and superconductivity [10] [2]. Spontaneous global symmetry breaking was introduced into four-dimensional, relativistic particle physics by Nambu [11], providing insight into the lightness of the pion and spontaneous chiral symmetry breaking. Subsequently, a simple field-theoretical model was formulated by Goldstone [12], and the appearance and number of massless scalar bosons appearing in such theories was specified by a theorem proved in [13]. In parallel, Nambu [14] and Anderson [15]

[2] The wheel has turned full circle with their importance for the construction of the LHC!

had shown how to interpret superconductivity in terms of a spontaneously-broken local U(1) symmetry. Moreover, Anderson had conjectured that this could occur also in the four-dimensional case, but Gilbert [16] argued in early 1964 that this would be impossible in a relativistic theory.

However, later in 1964 several papers successfully introduced spontaneously-broken local symmetry into particle physics. The initial paper by Englert and Brout [17] was followed a few weeks later by two papers written by Higgs, who did not know about their work at the time. The first Higgs paper [18] pointed out that Gilbert's objection to a four-dimensional extension of Anderson's approach could be circumvented, and the second proposed a specific four-dimensional model with a massive scalar boson [19]. The subsequent paper by Guralnik, Hagen and Kibble [20] developed the ideas proposed in these earlier papers. Also of note is a relatively-unknown 1965 paper by Migdal and Polyakov [21], which discusses the partial breaking of a local non-Abelian symmetry, ahead of the influential paper of Kibble [22].

Of all these authors, Higgs was the only one who mentioned explicitly the existence of a massive scalar boson (see equation (2b) of his second paper [19]), and he went on to write a third paper in 1966 [23] that discusses the properties of this 'Higgs boson' in surprising detail including, e.g., its decays into massive vector bosons.

1.4 Spontaneous Symmetry-Breaking in a U(1) Model

As an illustration of spontaneous symmetry breaking [24], consider first a single complex scalar field $\phi = \phi_1 + \phi_2$ with the following effective potential:

$$V\left(\phi^*\phi\right) = \mu^2\left(\phi^*\phi\right) + \lambda\left(\phi^*\phi\right)^2 \ , \tag{5}$$

where μ^2 and $\lambda > 0$ are real constants. This Lagrangian is clearly invariant under global U(1) phase transformations

$$\phi \to e^{i\alpha}\phi \ , \tag{6}$$

where α is a phase (rotation) angle. If the parameter μ^2 in (5) is positive, there is a unique vacuum state with $\langle\phi\rangle = 0$. Perturbing around this vacuum reveals that, in this case, ϕ_1 and ϕ_2, have the same mass. The symmetry of the original Lagrangian is explicit in this case.

Consider now the case $\mu^2 < 0$, corresponding to the 'Mexican Hat' potential illustrated in Fig.1. When we minimize the potential (5) we find a non-zero vacuum expectation value, or v.e.v., of the scalar field with:

$$|\phi|^2 \ = \ \phi_1^2 + \phi_2^2 \ = \ -\frac{\mu^2}{2\lambda} \ , \tag{7}$$

and the phase α undetermined. Thus, when $\mu^2 < 0$ there is a set of equivalent minima lying around a circle of radius $\sqrt{-\mu^2/\left(2\lambda\right)}$, and choosing one of them breaks the rotational symmetry spontaneously.

The U(1) symmetry is now implicit, since it relates the different equivalent vacua, corresponding to the appearance of spontaneous symmetry breaking. In order to see the particle content, we choose, without loss of generality, a particular ground state around which to perturb:

$$\phi_{1,\text{vac}} = \sqrt{-\frac{\mu^2}{2\lambda}} \equiv \frac{v}{\sqrt{2}} \quad , \quad \phi_{2,\text{vac}} = 0 \ . \tag{8}$$

The perturbations may be parametrized by

$$\frac{\eta}{\sqrt{2}} \equiv \phi_1 - \frac{v}{\sqrt{2}} \quad , \quad \frac{\xi}{\sqrt{2}} \equiv \phi_2 \ , \tag{9}$$

so that $\phi = \left(v + \eta + i\xi\right)/\sqrt{2}$, where η and ξ are real fields. In terms of these, the effective potential becomes

$$\mathcal{L} \ = \ -\frac{\mu^2}{2}\eta^2 - \frac{\lambda}{2}\left[\left(v+\eta\right)^2 + \xi^2\right]^2 - \mu^2 v\eta - \frac{\mu^2}{2}\xi^2 - \frac{1}{2}\mu^2 v^2 \ .$$

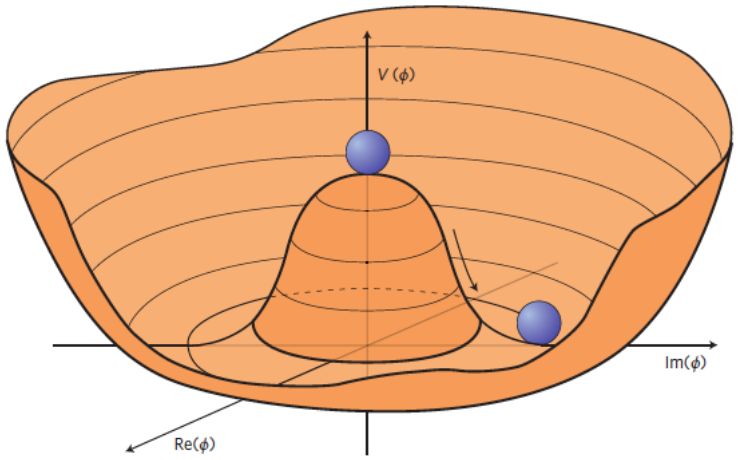

Fig. 1: An illustration of the Higgs potential (5) in the case that $\mu^2 < 0$, in which case the minimum is at $|\phi|^2 = -\mu^2/(2\lambda)$. Choosing any of the points at the bottom of the potential breaks spontaneously the rotational U(1) symmetry.

The scalar particle corresponding to η is massive with $m_\eta^2 = -\mu^2 > 0$, whereas the scalar particle corresponding to ξ is massless.

This particle is a prototype of a (Nambu-)Goldstone boson. It is massless because there is a direction in field space, corresponding to changing the phase, in which the potential energy does not change. Its appearance is a general feature of models with spontaneously-broken global symmetries, as proven in [13]. The total number of such massless particles corresponds in general to the number of field directions in which the potential is flat. Nambu introduced this idea into particle physics in order to describe the (relatively light) pion of QCD [11], which he identified as a (pseudo-)Goldstone boson of chiral symmetry that would have no mass if the up and down quarks were exactly massless. The simple field-theoretical model is due to Goldstone [12].

We now discuss how this spontaneous symmetry breaking of symmetry manifests itself in the presence of a U(1) gauge field [17, 19, 20]. In order to construct a theory that is invariant under local U(1) phase transformations, i.e.

$$\phi \to e^{i\alpha(x)}\phi \,, \tag{10}$$

we introduce a gauge field $\mathcal{A}_\mu$ that transforms under U(1) as follows:

$$\mathcal{A}'_\mu \to \mathcal{A}_\mu + \frac{1}{q}\partial_\mu \alpha\,(x) \ . \tag{11}$$

The space-time derivatives appearing in the kinetic term for the scalar field ϕ are replaced by covariant derivatives

$$D_\mu = \partial_\mu + iq\mathcal{A}_\mu \,, \tag{12}$$

where q is the conserved charge. Including kinetic terms for both the scalar field and the $\mathcal{A}_\mu$ field: $(1/4)\,F^{\mu\nu}F_{\mu\nu}$ where $F_{\mu\nu} \equiv \partial_\nu \mathcal{A}_\mu - \partial_\mu \mathcal{A}_\nu$, which is invariant under the U(1) gauge transformation (11), we have the Lagrangian

$$\mathcal{L} = \left[\left(\partial_\mu - iq\mathcal{A}_\mu\right)\phi^*\right]\left[\left(\partial^\mu + iq\mathcal{A}^\mu\right)\phi\right] - V\left(\phi^*\phi\right) - \frac{1}{4}F^{\mu\nu}F_{\mu\nu} \,, \tag{13}$$

which we now analyze.

We minimize the potential $V(\phi)$ as before, and write the Lagrangian in terms of the perturbations around the ground state (9):

$$\begin{aligned}\mathcal{L} &= \left\{\frac{1}{2}\left[(\partial^\mu\eta)(\partial_\mu\eta) - \mu^2\eta^2\right] + \frac{1}{2}(\partial^\mu\xi)(\partial_\mu\xi) - \frac{1}{4}F^{\mu\nu}F_{\mu\nu} + \frac{1}{2}q^2v^2\mathcal{A}^\mu\mathcal{A}_\mu\right\} \\ &+ vq^2A^\mu\mathcal{A}_\mu\eta + \frac{q^2}{2}\mathcal{A}^\mu\mathcal{A}_\mu\eta^2 + q(\partial^\mu\xi)\mathcal{A}_\mu(v+\eta) - q(\partial^\mu\eta)\mathcal{A}_\mu\xi \\ &- \mu^2v\eta - \frac{\mu^2}{2}\xi^2 - \frac{\lambda}{2}\left[(v+\eta)+\xi^2\right]^2 - \frac{\mu^2v}{2}\,. \end{aligned} \tag{14}$$

As before, the first three terms describe a (real) scalar particle, η, with mass $\sqrt{-\mu^2}$ and a massless Goldstone boson, ξ. The fourth term describes the free U(1) gauge field. However, whereas previously the Lagrangian (13) apparently described a massless gauge boson field, we now see in the spontaneously-broken phase (14) a term proportional to $\mathcal{A}_\mu\mathcal{A}^\mu$, corresponding to a mass for the gauge field:

$$m_{\mathcal{A}} = qv\,, \tag{15}$$

that is proportional to the vacuum expectation value of the Higgs field.

The other terms in (14) describe couplings between the fields A^μ, η and ξ, including a bilinear interaction coupling $\propto A^\mu\partial_\mu\xi$. The correct particle interpretation of (14) is obtained by diagonalizing the bilinear terms, which is easily done by using the gauge freedom of $\mathcal{A}_\mu$ to replace

$$\mathcal{A}_\mu \to \mathcal{A}'_\mu = \mathcal{A}_\mu + \frac{1}{qv}\partial_\mu\xi\,, \tag{16}$$

and making the local phase transformation

$$\phi \to \phi' = e^{-i\xi(x)/v}\phi = \frac{v+\eta}{\sqrt{2}}\,. \tag{17}$$

Following this transformation, the field ξ disappears, and (14) takes the simple form

$$\mathcal{L} = \frac{1}{2}\left[(\partial^\mu\eta)(\partial_\mu\eta) - \mu^2\eta^2\right] - \frac{1}{4}F^{\mu\nu}F_{\mu\nu} + \frac{q^2v^2}{2}\mathcal{A}^{\mu\,\prime}\mathcal{A}'_\mu + \ldots\,. \tag{18}$$

where the ... represent trilinear and quadrilinear interactions.

The Goldstone boson ξ that appeared when the global U(1) symmetry was broken spontaneously by the choice of ground state when $\mu^2 < 0$ has been absorbed (or 'eaten') by the gauge field $\mathcal{A}_\mu$, which thereby acquired a mass. Remember that, whereas a massless gauge boson has only two degrees of freedom (transverse polarization states), a massive gauge boson has a third (longitudinal) polarization state that is supplied by the Goldstone boson of the spontaneously-broken U(1) global symmetry. This is the Englert-Brout-Higgs mechanism.

In order for this mechanism to work, the magnitude of the v.e.v. of the scalar field must be fixed dynamically, which occurs in this model because the potential varies non-trivially in the radial ($|\phi|$) direction. The mass term for the η field in (18) is a reflection of this variation in the potential. The appearance of such a massive scalar boson is an unavoidable signature of spontaneous symmetry breaking.

1.5 Spontaneous Symmetry Breaking in the Standard Model

As already mentioned, the gauge group of the Standard Model is $SU(2)_L \times U(1)_Y$ [3, 4, 7], and the Lagrangian can be written in the form

$$\mathcal{L} = \mathcal{L}_{\text{gauge}} + \mathcal{L}_{\text{leptons}}$$

$$\begin{aligned}\mathcal{L}_{\text{gauge}} &= -\frac{1}{4}F^a_{\mu\nu}F^{a\mu\nu} - \frac{1}{4}f_{\mu\nu}f^{\mu\nu} \\ \mathcal{L}_{\text{leptons}} &= \overline{\mathrm{R}}\left(\partial_\mu + i\frac{g'}{2}\mathcal{A}_\mu Y\right)\mathrm{R} + \overline{\mathrm{L}}i\gamma^\mu\left(\partial_\mu + i\frac{g'}{2}\mathcal{A}_\mu Y + i\frac{g}{2}\tau\cdot\mathbf{B}_\mu\right)\mathrm{L}\,,\end{aligned} \tag{19}$$

where the field-strength tensors, $F_{\mu\nu}$ and $f_{\mu\nu}$, were defined in (2) and (3), respectively, g is the SU(2) coupling and g' is the U(1) hypercharge coupling. The symbol L represents doublets of left-handed fermions and R represents right-handed fermions. As written in (19), the theory contains four massless bosons ($\mathcal{A}_\mu$, B^1_μ, B^2_μ, B^3_μ).

We now introduce a scalar field that is a complex doublet of SU(2) [3, 4]:

$$\phi = \begin{pmatrix} \phi^+ \\ \phi^0 \end{pmatrix}\,, \tag{20}$$

and add to the Lagrangian

$$\mathcal{L}_{\text{Higgs}} = \left(D_\mu\phi\right)^\dagger\left(D^\mu\phi\right) - V\left(\phi^\dagger\phi\right)\,, \tag{21}$$

with an effective potential of similar form to (5):

$$V\left(\phi^\dagger\phi\right) = \mu^2\left(\phi^\dagger\phi\right) + \lambda\left(\phi^\dagger\phi\right)^2\,, \tag{22}$$

with $\mu^2 < 0$ and $\lambda > 0$. We also include Yukawa interactions between this scalar field and the matter fermions:

$$\mathcal{L}_{\text{Yukawa}} = -G_e\left[\overline{\mathrm{R}}\phi^\dagger\mathrm{L} + \overline{\mathrm{L}}\phi\mathrm{R}\right]\,, \tag{23}$$

which yield masses for the matter fermions, as we see later.

As in the U(1) case when $\mu^2 < 0$, $\langle\phi\rangle = 0$ is an unstable local maximum of the effective potential. The minimum has $\langle\phi\rangle \neq 0$ with an arbitrary SU(2)×U(1) orientation, leading to spontaneous symmetry breaking. Minimizing the effective potential as in the U(1) case, we obtain

$$\frac{\partial}{\partial\left(\phi^\dagger\phi\right)}V\left(\phi^\dagger\phi\right) = \mu^2 + 2\lambda\langle\phi\rangle_0 = \mu^2 + 2\lambda\left[\left(\phi^+_{\text{vac}}\right)^2 + \left(\phi^0_{\text{vac}}\right)^2\right] = 0\,. \tag{24}$$

Without loss of generality, we may set $\phi^+_{\text{vac}} = 0$ and take $\phi^0_{\text{vac}} = \sqrt{-\mu^2/\left(2\lambda\right)}$. This choice breaks both the SU(2) and U(1) symmetries, but preserves invariance under a residual U(1) gauge symmetry that we may identify with electromagnetism. Since three of the four generators are broken spontaneously by the v.e.v., the spectrum of the global theory would contain three massless (Nambu-)Goldstone bosons.

To see how these are 'eaten' by three of the gauge bosons, we consider perturbations around the chosen vacuum, representing the scalar field as

$$\phi = \exp\left(\frac{i\xi\cdot\tau}{2v}\right)\begin{pmatrix} 0 \\ \left(v+\eta\right)/\sqrt{2} \end{pmatrix}\,. \tag{25}$$

Just as in the U(1) case discussed in the previous section where we rotated away the Goldstone boson ξ, we are able in this case to make the following gauge transformation on the scalar ϕ and the gauge and matter fields:

$$\phi \;\rightarrow\; \phi' = \exp\left(\frac{-i\xi\cdot\tau}{2v}\right)\phi = \begin{pmatrix} 0 \\ \left(v+\eta\right)/\sqrt{2} \end{pmatrix}\,. \tag{26}$$

$$\tau\cdot\mathbf{B}_\mu \;\rightarrow\; \tau\cdot\mathbf{B}'_\mu \tag{27}$$

$$\mathrm{L} \;\rightarrow\; \mathrm{L}' = \exp\left(\frac{-i\xi\cdot\tau}{2v}\right)\mathrm{L}\,, \tag{28}$$

where τ is an SU(2) matrix, which leaves $\mathcal{A}_\mu$ and R invariant.

In this unitary gauge, and henceforward simplifying the notation: $\phi' \to \phi$, etc., so that

$$\phi = \begin{pmatrix} 0 \\ (v+\eta)/\sqrt{2} \end{pmatrix} , \tag{29}$$

and

$$\phi^\dagger \phi = \left(\frac{v+\eta}{\sqrt{2}} \right)^2 , \tag{30}$$

we see that

$$V\left(\phi^\dagger \phi\right) = \mu^2 \left(\frac{v+\eta}{\sqrt{2}} \right)^2 + \lambda \left(\frac{v+\eta}{\sqrt{2}} \right)^4 . \tag{31}$$

We also have

$$D_\mu \phi = \partial_\mu \phi + \frac{ig'}{2} \mathcal{A}_\mu Y \phi + \frac{ig}{2} \tau \cdot \mathbf{B}_\mu \phi \, , \tag{32}$$

which may be written in the form

$$D_\mu \phi = \begin{pmatrix} \frac{ig}{2} \left(\frac{v+\eta}{\sqrt{2}} \right) \left(B^1_\mu - i B^2_\mu \right) \\ \frac{1}{\sqrt{2}} \partial_\mu \eta + \left(\frac{v+\eta}{\sqrt{2}} \right) \frac{i}{2} \left(i g' \mathcal{A}_\mu - i g B^3_\mu \right) \end{pmatrix} \tag{33}$$

and hence

$$\left(D^\mu \phi\right)^\dagger \left(D_\mu \phi\right) = \frac{g^2}{8} (v+\eta)^2 \left| B^1_\mu - i B^2_\mu \right|^2 + \frac{1}{2} \left(\partial_\mu \eta\right) \left(\partial^\mu \eta\right) + \frac{1}{8} (v+\eta)^2 \left(g' \mathcal{A}_\mu - g B^3_\mu \right)^2 . \tag{34}$$

The final form of the scalar Lagrangian is therefore

$$\begin{aligned} \mathcal{L}_{\rm Higgs} &= \left\{ \frac{1}{2} \left(\partial_\mu \eta\right) \left(\partial^\mu \eta\right) - \frac{\mu^2}{2} \eta^2 + \frac{v^2}{8} \left[g^2 |B^1_\mu - i B^2_\mu|^2 + \left(g' \mathcal{A}_\mu - g B^3_\mu \right)^2 \right] \right\} \\ &+ \left\{ \frac{1}{8} \left(\eta^2 + 2v\eta \right) \left[g^2 |B^1_\mu - i B^2_\mu|^2 + \left(g' \mathcal{A}_\mu - g B^3_\mu \right)^2 \right] \right\} \\ &- \left\{ \frac{1}{4} \eta^4 - \lambda v \eta^3 - \frac{\mu^2}{2} \eta^2 - \left(\lambda v^3 + \mu^2 v \right) \eta - \left(\frac{\lambda v^4}{4} + \frac{\mu^2 v^2}{2} \right) \right\} , \end{aligned} \tag{35}$$

whose interpretation we now discuss.

The second term on the first line of (35) is a mass term for the η field: this is the Higgs boson, which appears in the same way as in the previous U(1) case. *A priori*, there is no theoretical prediction within the Standard Model for the Higgs mass

$$m_H = -2\mu^2 \, , \tag{36}$$

since μ is not determined by any of the known parameters of the Standard Model. The following terms on the first line of (35) are mass terms for the massive vector bosons, to which we return later. The second line includes interactions of the Higgs boson with these massive gauge bosons, and the last line describes self-interactions of the Higgs boson.

We define the charged gauge fields $W^\pm_\mu$ as the combinations

$$W^\pm_\mu \equiv \frac{B^1_\mu \mp i B^2_\mu}{\sqrt{2}} \, , \tag{37}$$

and identify the following neutral gauge boson mass eigenstates:

$$Z_\mu \equiv \frac{-g' \mathcal{A}_\mu + g B^3_\mu}{\sqrt{g^2 + g'^2}} \, , \tag{38}$$

$$A_\mu \equiv \frac{g\mathcal{A}_\mu + g' B^3_\mu}{\sqrt{g^2 + g'^{\,2}}} \,. \tag{39}$$

Substituting these expressions in the Lagrangian (35), we find

$$\mathcal{L}_{\text{Higgs}} = \left[\frac{1}{2}\left(\partial^\mu \eta\right)\left(\partial_\mu \eta\right) - \frac{\mu^2}{2}\eta^2\right] + \frac{v^2 g^2}{8} W^{+\,\mu} W^+_\mu + \frac{v^2 g^2}{8} W^{-\,\mu} W^-_\mu + \frac{\left(g^2 + g'^{\,2}\right) v^2}{8} Z^\mu Z_\mu + \ldots \,, \tag{40}$$

and it is evident that the field $\mathcal{A}_\mu$ is massless. This is due to the unbroken U(1) symmetry (i.e., the symmetry under $e^{iQ\alpha(x)}$ rotations) that we identify with electromagnetism. On the other hand, the charged vector bosons $W^\pm$ and the neutral vector boson Z^0 have masses

$$m_W = \frac{gv}{2} \quad , \quad m_Z = \frac{v}{2}\sqrt{g^2 + g'^{\,2}} \,. \tag{41}$$

We see that the couplings of the Higgs boson to the $W^\pm$ and Z^0 in (35) are related to these masses. They are related through

$$m_Z = m_W \sqrt{1 + g'^{\,2}/g^2} \,. \tag{42}$$

It is convenient to introduce the angle θ_W to parametrize the mixing of the neutral gauge bosons, defined by

$$\tan\theta_W = \frac{g'}{g} \,, \tag{43}$$

so that

$$\cos\theta_W = \frac{g}{\sqrt{g^2 + g'^{\,2}}} \quad , \quad \sin\theta_W = \frac{g'}{\sqrt{g^2 + g'^{\,2}}} \,. \tag{44}$$

Eqs. (38) and (39) can then be written as

$$Z_\mu = -\sin\theta_W \mathcal{A}_\mu + \cos\theta_W B^3_\mu \,, \tag{45}$$

$$A_\mu = \cos\theta_W \mathcal{A}_\mu + \sin\theta_W B^3_\mu \,, \tag{46}$$

and the relation (42) between the masses of $W^\pm$ and Z^0 becomes

$$m_W = m_Z \cos\theta_W \,. \tag{47}$$

The ratio

$$\rho \equiv \frac{m_W^2}{m_Z^2 \cos^2\theta_W} \tag{48}$$

is equal to unity at the tree level in the Standard Model. This is a direct consequence of the choice of isospin 1/2 for the Higgs field (20).

This choice also enables the Higgs field to give masses to the Standard Model fermions [3], as we now discuss. Looking at the fermion Lagrangian (23) in the unitary gauge, it becomes

$$\mathcal{L}_{\text{Yukawa}} = -G_e \left[\overline{e}_R \phi^\dagger \begin{pmatrix} \nu_L \\ e_L \end{pmatrix} + \left(\overline{\nu}_L \; \overline{e}_L\right) \phi e_R\right] = -G_e \frac{v+\eta}{\sqrt{2}} \left(\overline{e}_R e_L + \overline{e}_L e_R\right) \,. \tag{49}$$

In terms of $\overline{e} \equiv (\overline{e}_R, \overline{e}_L)$ and $e \equiv (e_L, e_R)^T$, (49) becomes

$$\mathcal{L}_{\text{Yukawa}} = -\frac{G_e v}{\sqrt{2}} \overline{e} e - \frac{G_e \eta}{\sqrt{2}} \overline{e} e \,, \tag{50}$$

and we see that the electron has a mass

$$m_e = G_e \frac{v}{\sqrt{2}} \,. \tag{51}$$

The same holds for all the Standard Model fermions, and their couplings to the Higgs boson are proportional to their masses. Thus, the Higgs boson prefers to decay into the heaviest fermions f that are kinematically accessible, i.e., have $m_f < m_H/2$.

At first sight, the Lagrangian (35) may look rather artificial. However, as described above, the spontaneous symmetry breaking mechanism for giving masses to vector bosons and fermions is in fact very generic. It suffices to have a scalar field ϕ and choose the coefficient μ^2 of the quadratic term in its effective potential to be negative, and the mass-generation mechanism follows automatically. The original Lagrangian (21) is in fact very symmetric, and this symmetry is still present, though hidden, in (35).

Since the theory (35) still possesses symmetry, it is a renormalizable theory at the quantum level [25], which enables many detailed calculations to be compared with precise experimental measurements. In fact, not only is it *a* renormalizable theory, it is *the only* way to construct a renormalizable theory of interacting massive vector bosons [26–28]. In order to get some flavour why this is the case, consider $W^+W^- \to W^+W^-$ scattering. At the tree level, the combination of γ and Z^0 exchanges in the direct and crossed channels with the point-like quartic coupling, shown in the two upper rows of Fig. 2, yields a scattering amplitude that grows quadratically with energy:

$$\mathcal{M}_V \; = -g^2 \frac{E^2}{m_W^2} + \mathcal{O}(E^0) \, . \tag{52}$$

This is a problem when one calculates loop diagrams, since the integral over the loop momenta is uncontrollably divergent. If one now includes a scalar with a coupling g_{HWW} to the vector bosons, the direct and crossed-channel scalar exchanges, shown in the bottom row of Fig. 2, yield an amplitude

$$\mathcal{M}_S \; = +g_{HWW}^2 \frac{E^2}{m_W^2} + \mathcal{O}(E^0) \, . \tag{53}$$

Adding these contributions, we find

$$\mathcal{M} \; = \; \mathcal{M}_V + \mathcal{M}_S \; = \; \frac{m_H^2}{v^2} \left(2 + \frac{m_H^2}{s - m_H^2} + \frac{m_H^2}{t - m_H^2} \right) + \ldots \, , \tag{54}$$

where the $\ldots$ represent terms that are subdominant at high energies, *iff* the HWW coupling coincides with the prediction from spontaneous symmetry breaking. The fact that the resultant amplitude $\mathcal{M}$ is asymptotically constant for this particular choice of g_{HWW} ensures that the integration over the loop momentum is controllable and permits the theory to be renormalizable [3] - which it is if the other particle couplings also coincide with the spontaneously-broken gauge theory.

1.6 A Phenomenological Profile of the Higgs Boson

1.6.1 Before the LHC

For a decade after the original papers after spontaneously-broken gauge theories were formulated, and even for several years after they were proven to be renormalizable, rather few people took seriously Higgs' prediction of the boson that bears his name. Indeed, only a handful of papers discussed its possible experimental signatures before the paper that Mary Gaillard, Dimitri Nanopoulos and I wrote in 1975 [29] with the same title as this Section heading. In the last sentence of our paper we wrote that "*we do not want to encourage big experimental searches for the Higgs boson*". Fortunately, the experimental community did not pay attention to this caveat, and the ATLAS and CMS experiments announced the discovery of a candidate for a (the?) Higgs boson on July 4th 2012 [1, 2].

[3] A similar argument applies to fermion-W scattering and the scalar-fermion coupling, which must also coincides with the prediction from spontaneous symmetry breaking.

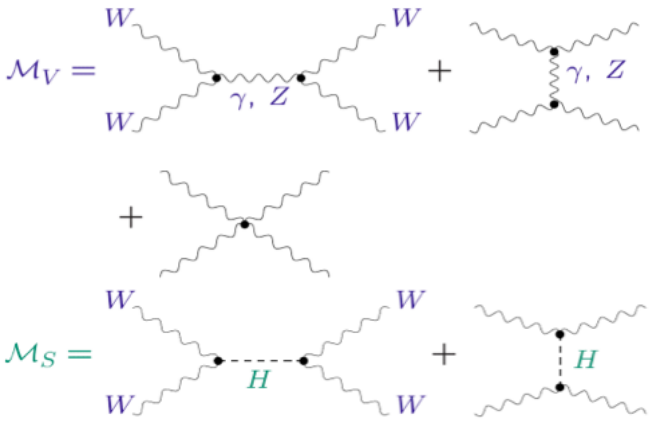

Fig. 2: Contributions to WW scattering from diagrams due to vector boson exchange and the four-point gauge interaction in the absence of a Higgs boson (upper two rows), and diagrams due to Higgs boson exchange (lowest row).

The search for the Higgs boson at LEP was advertized in the first survey of LEP physics made in 1976 [30] and featured strongly in the subsequent LEP experimental programme [31]. These direct searches for the Higgs boson resulted in the lower limit [32]

$$m_H \; > \; 114.4 \, \text{GeV} \, , \tag{55}$$

shown as the left-hand of the two yellow excluded regions in Fig. 3. The search for the Higgs boson was also advertized at the first LHC physics workshop in 1984 and grew subsequently to become one of the major objectives of the LHC experimental programme.

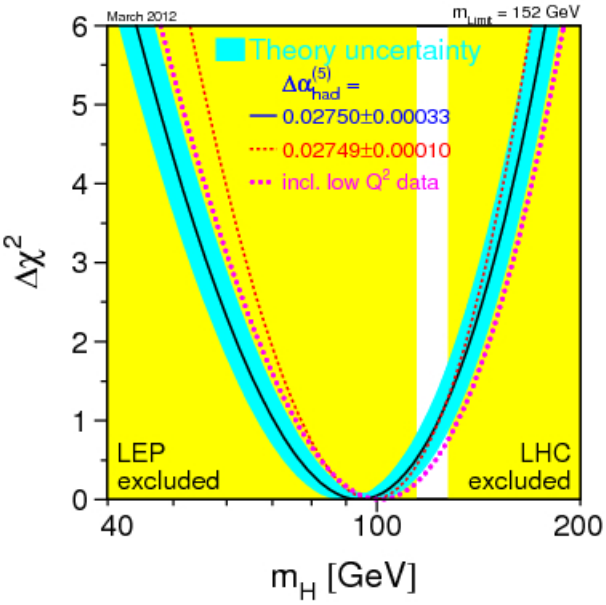

Fig. 3: The status of the Higgs search in March 2012 [8]. The left-hand yellow-shaded region is the LEP exclusion, and the right-hand yellow-shaded region is the Tevatron exclusion at that time [33].

Although LEP found no direct evidence for the Higgs boson, the precision of electroweak measurements at LEP and elsewhere provided indirect indications on the Higgs mass through the sensitivity of electroweak observables to quantum loop corrections. For example, there is a one-loop correction Δr

to the $W^{\pm}$ and Z^0 masses:

$$m_W^2 \sin^2\theta_W \;=\; m_Z^2 \cos^2\theta_W \sin^2\theta_W \;=\; \frac{\pi\alpha}{\sqrt{2}G_F}\,(1+\Delta r)\;. \tag{56}$$

The one-loop correction Δr and other electroweak radiative corrections are in turn sensitive to the masses of heavy virtual particles, in particular m_t and m_H:

$$\propto\; \frac{3G_F}{8\pi^2\sqrt{2}}m_t^2\;,\; \frac{\sqrt{2}G_F}{16\pi^2}\left(\frac{11}{3}\ln\frac{m_H^2}{m_Z^2}+\ldots\right) \tag{57}$$

in the limits of large m_t and $m_H \gg m_{W,Z}$. Note that the sensitivity to m_t is quadratic [34], whereas that to m_H is only logarithmic [35]. The large-mass divergences in (57) reflect the fact that the electroweak theory would become renormalizable if these particles were absent. In the case of the top quark, its absence would leave us with an incomplete fermion doublet, and the problems arising in the absence of the Higgs boson were discussed at the end of the previous Section.

First attempts to use precision measurements to constrain m_H were made before the discovery of the top quark [36], and already indicated that $m_H = \mathcal{O}(m_W)$. The discovery of the top quark with a mass consistent with predictions based on electroweak data and (56) enabled the prediction of m_H to be sharpened, as has the inclusion of QCD and higher-order electroweak effects, as illustrated by the blue band in Fig. 3.

A conservative estimate of the current estimate of m_H on the basis of precision electroweak data alone is [8, 9]

$$m_H \;=\; 100 \pm 30\ \mathrm{GeV}\,, \tag{58}$$

which is quite compatible with the direct lower limit (55) and the exclusion by the Tevatron of $m_H \sim 160$ to 170 GeV. Combining the LEP and Tevatron exclusions with the precision electroweak data led in mid-2011 to the prediction [37]:

$$m_H \;=\; 125 \pm 10\ \mathrm{GeV}\,. \tag{59}$$

This has been an impressively successful prediction!

1.6.2 Higgs Production at the LHC

Several production modes are measurable at the LHC for a Higgs boson weighing ~ 125 GeV, as displayed in Fig. 4 for Higgs production at the LHC at 8 TeV. The dominant mechanism is calculated to be gluon-gluon fusion: $gg \to H$ via loops of heavy coloured particles [38], of which the most important in the Standard Model is the top quark. Since the leading-order contribution to the production amplitude is $\mathcal{O}(\alpha_s)$, making an accurate calculation is particularly challenging. However, the cross section has been calculated by different theoretical groups at next-to-next-to-leading order (NNLO), including also the most important logarithms at higher orders (NNLL), with good agreement between the calculations as seen in Fig. 5 [39]. The main remaining uncertainties in the calculation are associated with the choice of renormalization scale in the calculation, and in the gluon parton distribution function within the proton. The overall theoretical uncertainty is currently estimated to be about 10%, and a significant rise in the cross section is expected when the LHC reaches 13/14 TeV in 2015.

The second-largest contribution to Higgs production at the LHC is due to vector-boson fusion (VBF) [40]. This has now been calculated at NNLO in α_s and including electroweak corrections at NLO, and the perturbation expansion is converging well. In this case, the uncertainties in quark parton distribution functions are relatively small, so this cross section is known more accurately, and it grows with energy more rapidly than gluon-gluon fusion [39].

The third-largest contribution is associated production of the Higgs with a massive vector boson $V = W^{\pm}, Z^0$ [41]. This has also been calculated at NNLO in α_s and including electroweak corrections

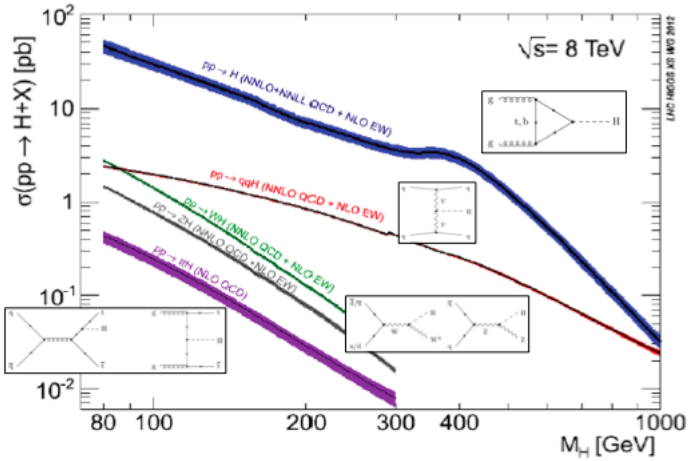

Fig. 4: The principal Higgs production cross sections at the LHC at 8 TeV. The insets depict the corresponding fundamental production subprocesses.

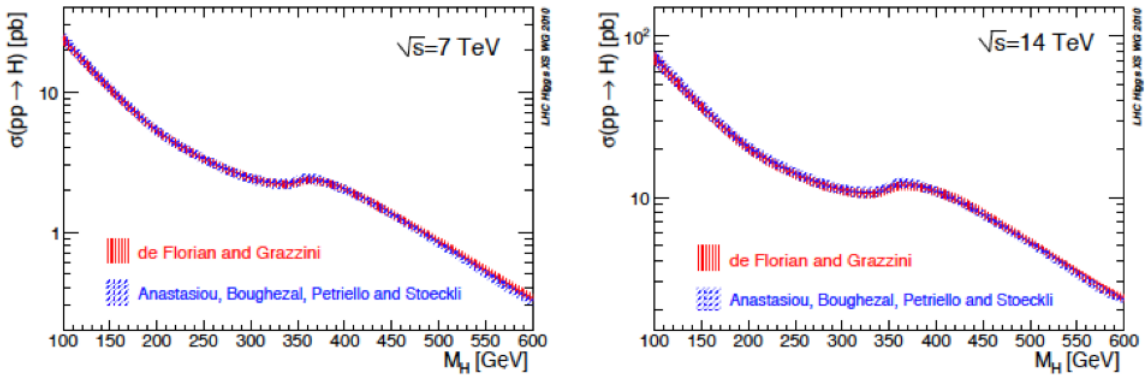

Fig. 5: The cross sections for $gg \to H$ production at the LHC at 7 and 14 TeV, comparing two next-to-next-leading order (NNLO) calculations that also include leading higher-order logs (NNLL) [39].

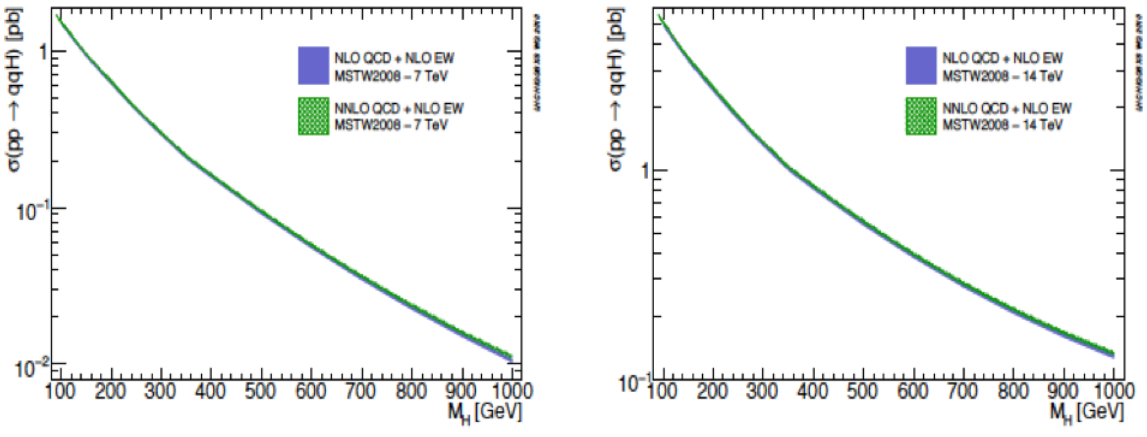

Fig. 6: The cross sections for VBF production of the H at the LHC at 7 and 14 TeV, comparing calculations at NLO in the electroweak interactions and at NLO and NNLO in QCD [39].

at NLO, as seen in the left panel of Fig. 7. and the perturbation expansion again converges well. Here the rate of growth of the cross section is less rapid.

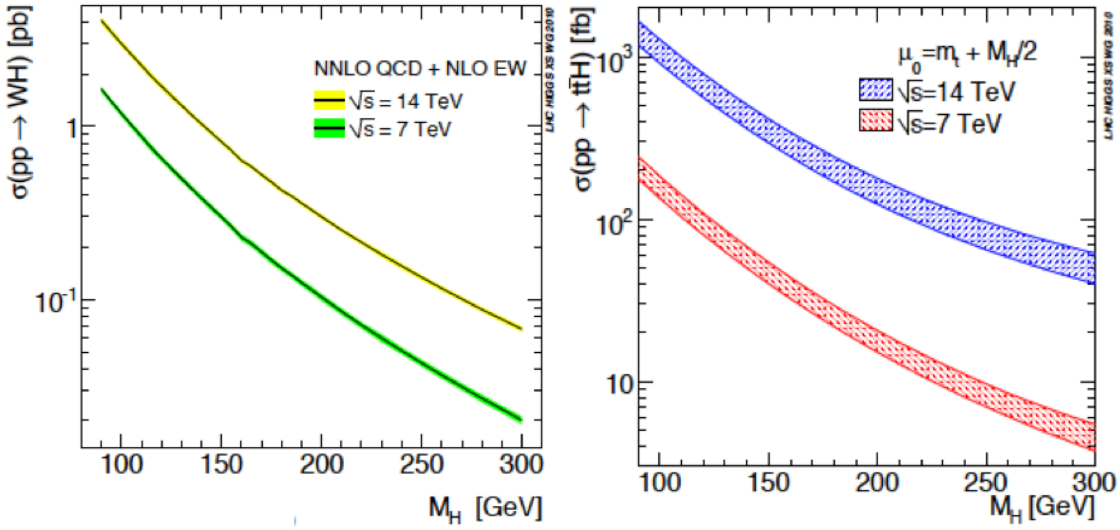

Fig. 7: The cross sections for production of the H in association with a massive vector boson V (left panel) and in association with $\bar{t}t$ (right panel) at the LHC at 7 and 14 TeV [39].

The next contribution is from associated $\bar{t}t + H$ production, which is currently known less accurately: it has been calculated at NLO in α_s, so there are larger uncertainties in the perturbation expansion, and the choice of parton distributions is also an important uncertainty [39]. This process has the most rapid cross section increase with energy, as seen in the right panel of Fig. 7, offering interesting prospects for measurement at LHC 13/14.

Finally, interest has recently been attracted by H production in association with a single t or $\bar{t}$ [42]. This has a relatively small cross section in the Standard Model, but it may be enhanced or suppressed significantly in models where the $H\bar{t}t$ coupling differs from its Standard Model value [43, 44], as we discuss later.

LHC experimentalists are indeed fortunate that all of these mechanisms are potentially measurable at the LHC for $m_H \sim 125$ GeV! This would not have been the case if the Higgs mass had been 400 GeV, say, in which case only $gg \to H$ and VBF could have been measurable.

1.6.3 Higgs Decays [45]

The Higgs decay rate into a pair of fermions is given at the tree level by

$$\Gamma(H \to \bar{f}f) \; = \; N_c \frac{G_F m_H}{4\pi\sqrt{2}} m_f^2 \,, \tag{60}$$

where $N_c = 3(1)$ for decays into quarks (leptons). Since the tree-level Higgs couplings to other particles are proportional to their masses (squared in the cases of massive vector bosons), the dominant Higgs decays are into the heaviest particles that are kinematically accessible. This implies that the dominant two-body decays of the Higgs weighing ~ 125 GeV are expected to be into $\bar{b}b$, $\bar{c}c$ and $\tau^+\tau^-$, as seen in the left panel of Fig. 8. However, decays into $\bar{b}b$ have yet to confirmed, there is no evidence for $\bar{c}c$, and $H \to \tau^+\tau^-$ decay has only recently has the been observed unambiguously [46].

The H decay rate into a pair of $W^\pm$ bosons, one on- and one off-shell, is given by

$$\Gamma(H \to WW^*) \; = \; \frac{G_F m_H^3}{8\pi\sqrt{2}} F(r) \,, \tag{61}$$

where $F(r \equiv m_W/m_H)$ is a kinematic factor, and the corresponding decay into a pair of Z bosons is given by a similar formula with $m_W \to m_Z$ and a symmetry factor of 1/2 [45]. The decays $H \to$ virtual

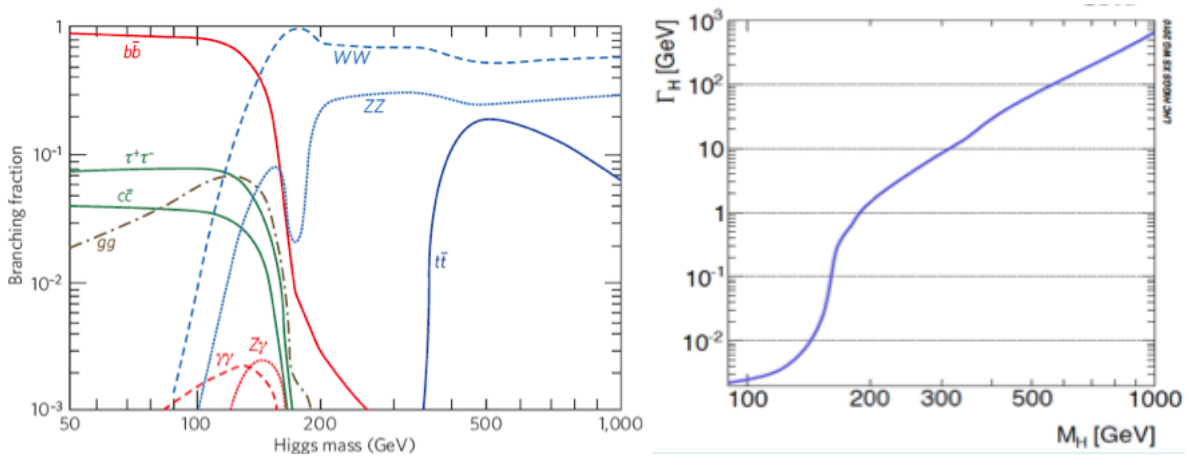

Fig. 8: The most important decay branching fractions for the decays of a Standard Model Higgs boson (left panel), and the total decay rate Γ_H (right panel) [45].

W^+W^- and Z^0Z^0 are important for $m_H \sim 125$ GeV, as seen in the left panel of Fig. 8, despite the fact that $m_H < 2m_W$ and $2m_Z$.

Moreover, although the decays $H \to gg$ and $\gamma\gamma$ are absent at the tree level, they are generated by quantum loops, as discussed above in connection with $gg \to H$ production. The dominant contributions to the $H \to \gamma\gamma$ decay amplitude are due to massive charged particles [29], the most important in the Standard Model being the t quark and the $W^\pm$ boson, whose contributions interfere destructively. At the one-loop level

$$\Gamma(H \to \gamma\gamma) = \frac{G_F \alpha^2 m_H^3}{128\pi^3\sqrt{2}} \left|\Sigma_f N_c Q_f^2 A_{1/2}(r_f) + A_1(r_W)\right|^2 , \tag{62}$$

where $A_{1/2}$ and A_1 are known functions of $r_f \equiv m_f/m_H$ and $r_f \equiv m_W/m_H$ that have opposite signs [45].

Decays into strongly-interacting final states have been evaluated at NNNLO in α_s, while electroweak decays have been evaluated at NLO. The total Higgs decay rate in the Standard Model is expected to be ~ 4.2 MeV for $m_H \sim 125$ GeV, as seen in the right panel of Fig. 8 [45].

Once again, Nature has been kind in her choice of the Higgs mass, with half-a-dozen Higgs decays being observable at the LHC for $m_H \sim 125$ GeV. If the Higgs mass had been 300 GeV, say, only the decays $H \to W^+W^-$ and Z^0Z^0 would have been measurable.

1.6.4 From Discovery to Measurement

Following the dramatic announcements of the discoveries of the Higgs boson by the ATLAS and CMS Collaborations on July 4th, 2012 [1, 2], the emphasis is now on measurements and the information they provide about physics within and beyond the Standard Model.

The strengths of the signals observed in many channels are compatible with the Standard Model predictions [47]. However, the bulk of the evidence concerns production by gluon-gluon fusion. There have been several observations of VBF channels at the 2-σ level, and the overall significance of the evidence for VBF is some 3 σ. So far the best evidence for production in association with massive vector bosons comes from the CDF and D0 experiments at the Fermilab Tevatron, and there are only upper limits on production in association with $\bar{t}t$.

The primary evidence for H decays is in final states involving vector bosons: $ZZ^*, \gamma\gamma$ and WW^*, whereas the direct evidence for decays into fermions is much weaker. Concerning leptons, although evidence for $H \to \tau^+\tau^-$ decay is emerging [46], but there are only upper limits on the decay into

$\mu^+\mu^-$ [47] (which may be the only second-generation final state accessible at the LHC) [4], and the prospects for measuring the He^+e^- coupling look very dim. Concerning quarks, evidence for $H \to \bar{b}b$ decay is also emerging, but there is only indirect evidence for an $H\bar{t}t$ coupling via measurements of $gg \to H$ production and $H \to \gamma\gamma$ decay. In the future, more information could be provided by $H \to Z^0\gamma$ decay and H production in association with a single t or $\bar{t}$ [42–44], as well as $H\bar{t}t$ production.

1.6.5 The Higgs Mass - Evidence for Physics beyond the Standard Model?

There are two ways to measure the Higgs mass accurately with the present data: using $H \to ZZ^* \to 4\ell^\pm$ and $\gamma\gamma$ decays. In the case of CMS, these two final states yield very similar masses, with $m_{\gamma\gamma}$ slightly lower. In the case of ATLAS, there is some tension between the measurements in the two channels, with $m_{\gamma\gamma}$ higher by ~ 2 GeV, corresponding to a ~ 2-σ discrepancy. However, the CMS and ATLAS measurements [47] are quite consistent, and a naive global average is

$$m_H \;=\; 125.6 \pm 0.4 \text{ GeV} . \tag{63}$$

As seen in Fig. 9, this is consistent at the $\Delta\chi^2 \sim 1.5$ level with the estimate of m_H provided by precision electroweak data [9]. A victory for the Standard Model at the quantum (loop) level!

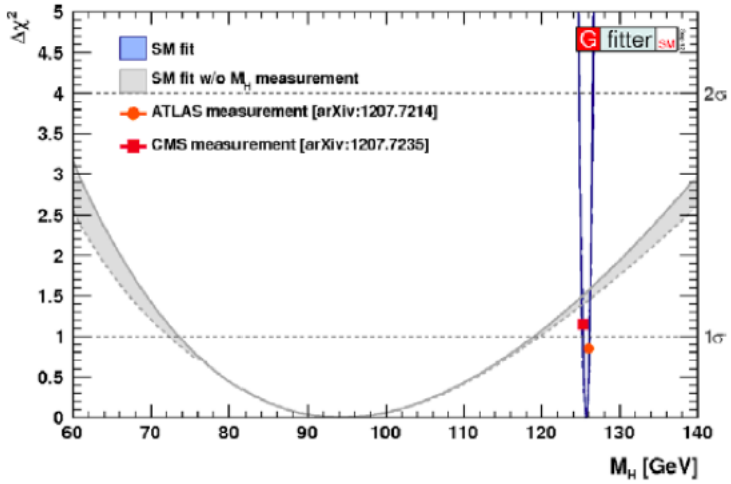

Fig. 9: Comparison of the indirect estimate of the Higgs mass based on precision electroweak data with the direct measurement by ATLAS and CMS [9].

However, issues arise when we consider the effective Higgs potential. There are two important sources of renormalization of the quartic Higgs self-coupling λ: that due to the Higgs self-coupling itself:

$$\lambda(Q) \;=\; \frac{\lambda(v)}{1 - \frac{3}{4\pi^2}\lambda(v)\ln\frac{Q^2}{v^2}} + \ldots , \tag{64}$$

where Q is some renormalization scale above the electroweak scale v, and that due to the $H\bar{t}t$ coupling:

$$\lambda(Q) \;=\; \lambda(v) - \frac{3m_t^4}{4\pi^2 v^4}\ln\frac{Q^2}{v^2} + \ldots , \tag{65}$$

where in each case the $\ldots$ represent subleading terms in the solution of the renormalization-group equation. We see in (64) that the self-renormalization tends to increase λ as Q increases, leading to an

[4] It would also be interesting to search for the flavour-changing decays $H \to \tau\mu$ and τe. These are highly suppressed in the Standatd Model, but model-independent upper bounds from low-energy flavour-changing processes allow these decays to occur at rates similar to $H \to \tau^+\tau^-$ [48].

apparent singularity (a so-called Landau pole). On the other hand, the renormalization by the t quark tends to reduce λ as Q increases, potentially driving it negative at some scale above v.

This would imply an instability in the electroweak vacuum if [49]

$$m_H \; < \; \left[129.4 + 1.4\left(\frac{m_t - 173.1\ \mathrm{GeV}}{0.7}\right) - 0.5\left(\frac{\alpha_s(m_Z) - 0.1184}{0.0007}\right) \pm 1.0_{\mathrm{TH}}\right]\ \mathrm{GeV}\,. \qquad (66)$$

The measured values of $m_t \sim 173$ GeV and m_H (63) would drive the quartic Higgs self-coupling negative at some scale $\sim 10^{10}$ to 10^{14} GeV, as seen in the left panel of Fig. 10, if no physics beyond the Standard Model intervenes at some lower energy scale. (One example of possible new physics is supersymmetry, to which we return later.) However, the lifetime of the vacuum is estimated to be probably much longer than the age of the Universe, as seen in the right panel of Fig. 10, so it is not an immediate issue for the future of humanity, leading some people to suggest that this instability is not a problem. My own point of view is that such an instability would make it much more difficult to understand why the current vacuum energy (cosmological constant) is so close to zero in natural units. Why should our present vacuum energy be small if we are in a temporary state on the way to a state with vacuum energy much larger in magnitude than now (and negative)?

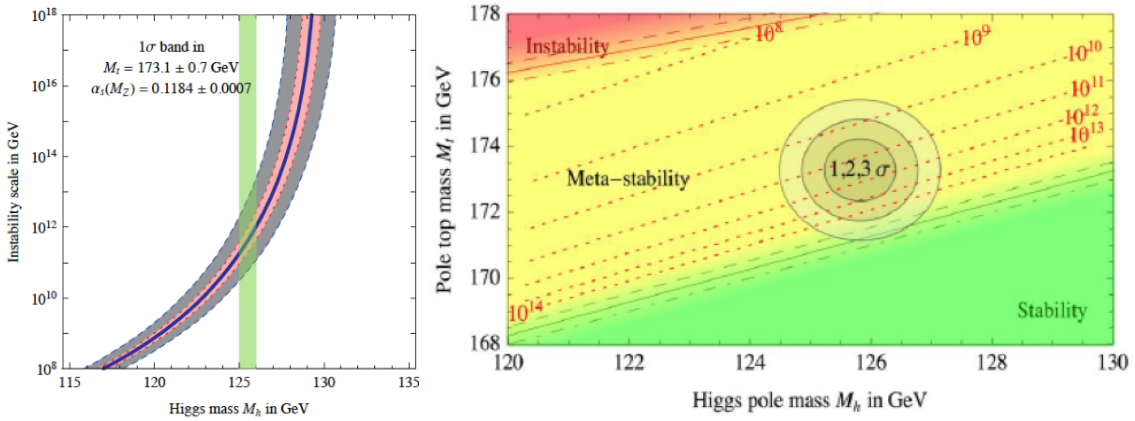

Fig. 10: Negative renormalization of the Higgs self-coupling by the top quark is calculated within the Standard Model to lead to an instability in the effective Higgs potential for field values $\sim 10^{13}$ to 10^{14} GeV (left panel). The current estimates of m_t and m_H suggest that the current electroweak vacuum is in fact metastable (right panel), though a definite conclusion must wait a more accurate measurement of m_t, in particular. Figures taken from [49].

It should be emphasized, however, that the conclusion that the electroweak vacuum is unstable is not definite, even within the Standard Model. The stability or otherwise of the electroweak vacuum depends sensitively on m_t as well as m_H (and. to a lesser extent, α_s). In addition to the quoted experimental error in m_t, there is also a theoretical uncertainty associated with the way m_t is defined and introduced into experimental Monte Carlo programmes [50], which warrants more study.

1.6.6 The Higgs Discovery is a Big Deal

As already mentioned, without the Higgs boson (or something to replace it), there would be no atoms, because massless lectrons would escape from nuclei at the speed of light without forming atoms, and the weak interactions would not be weak, everything would be radioactive, and life would be impossible. The discovery of a/the Higgs boson tells us how gauge symmetry is broken and whether there is such a thing as an elementary scalar field. it is likely to be the portal to new physics such as dark matter. The switch-on of the Higgs v.e.v. would have caused a phase transition in the Universe when it was about 10^{-12} seconds old, and may have played a role then in generating the matter in the Universe via electroweak baryogenesis. A related inflaton might have made the Universe expand exponentially when it was about 10^{-35} seconds old, and might contribute 10^{60} too much to today's dark energy!

2 What we know now

2.1 The Particle Jigsaw Puzzle

Fig. 11 summarizes our state of knowledge concerning the H signal strengths in the various different final states: $\bar{b}b, \tau^+\tau^-, \gamma\gamma, WW^*$ and ZZ^*, averaged over the results of ATLAS, CMS and the Tevatron experiments. The signal strengths in different production channels are presented (in blue), followed by the global combinations in each final state (in black). The combined mean signal strength in all channels (in red) is

$$\mu \;=\; 1.02^{+0.11}_{-0.12}\,, \tag{67}$$

and finally the combination of the signal strengths in the VBF and associated $V + H$ channels is shown (in green). We see that there is no indication of any significant deviation from the Standard Model predictions: Peter Higgs should be smiling!

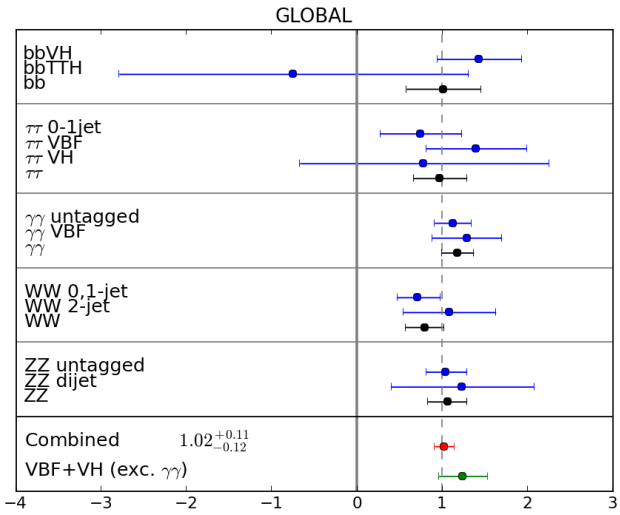

Fig. 11: A compilation of the Higgs signal strengths measured by the ATLAS, CDF, D0 and CMS Collaborations in the $\bar{b}b$, $\tau^+\tau^-$, $\gamma\gamma$, WW^* and ZZ^* final states. We display the combinations of the different channels for each final state, and also the combination of all these measurements, with the result for the VBF and VH channels (excluding the $\gamma\gamma$ final state) shown separately in the bottom line. Figure taken from [51].

The current situation of particle physicists resembles that of someone who has spent more than 100 years putting together a jigsaw puzzle, and has finally (after 48 years) discovered what may be the last missing piece, hidden away in the back of the sofa and with the picture rubbed off. Have the LHC experiments really discovered the missing piece, or is it an impostor? Does it have the right shape to fit into the empty space in the puzzle, and does it have the right size?

The rest of this lecture is devoted to answering these questions as best we can on the basis of the present data.

2.2 Is it the Missing Piece?

2.2.1 Does it have Spin 0 or 2?

The question 'does the newly-discovered H particle have the right shape to be the missing piece of the puzzle?' can be parsed as the question 'what is its spin?' Since the H particle decays into pairs of photons - identical spin-1 bosons - it must have some spin $\neq 1$. The simplest possibilities are spin 0 and 2, the Standard Model being an example of the former case, a Kaluza-Klein graviton being an example

of the second case. A higher spin cannot be excluded *a priori*, but I am unaware of any model with spin > 2.

Several ways to diagnose the H spin have been proposed, including the characteristics of production in association with $W^{\pm}$ or Z^0 [52, 54], the angular distribution of $\gamma\gamma$ decays [55, 56], and the kinematic correlations of leptons in WW^* and ZZ^* decays [57]. In general, a massive spin-2 particle has many possible couplings to Standard Model particles, and distinguishing the spin-0 and general spin-2 hypotheses is difficult. Here we consider the simplest spin-2 case (see [58] and references therein), in which it has minimal graviton-like couplings, as in simple models with extra dimensions:

$$\mathcal{L}_{int} \; = \; \Sigma_i \frac{c_i}{M_{eff}} G^{\mu\nu} T^i_{\mu\nu} \, , \tag{68}$$

where the sum is over Standard Model particle types i and the overall mass scale and the individual coefficients c_i are model-dependent.

For definiteness, we can consider warped compactifications of 5-dimensional theories [58], in which the metric takes the form:

$$ds^2 \; = \; w(z)^2 \left(\eta_{\mu\nu} dx^\mu dx^\nu - dz^2 \right) \, . \tag{69}$$

In such a scenario we expect identical coefficients for the couplings of a spin-2 particle X to the massless vector bosons g and γ:

$$c_g \; = c_\gamma \; = \; 1 / \int_{z_{UV}}^{z_{IR}} w(z) dz \, . \tag{70}$$

since their wave functions are uniform in the extra dimension. This implies the following simple relation between the decay rates of a spin-2 particle X into photons and gluons:

$$\Gamma(X \to gg) \; = \; 8 \Gamma(X \to \gamma\gamma) \, , \tag{71}$$

which is disfavoured by the data on the $H(126)$ decay branching ratios, as seen in Fig. 12. The couplings of the other Standard Model particles are non-universal, reflecting their different wave functions in the extra dimension. In simple warped compactifications one expects

$$c_b \; \simeq \; c_t \gtrsim \; c_W \simeq \; c_Z \; = \mathcal{O}(35) \times (c_g = c_\gamma > c_{u,d}) \; . \tag{72}$$

The experimental data on $H(126)$ decays also disfavour the expected hierarchy (72) between $c_W \simeq c_Z$ and $c_g = c_\gamma$, as also seen in Fig. 12 [5].

The difference between the spin-2 couplings (69) and spin-0 couplings also affect the kinematics of production in association with massive vector bosons $W^{\pm}$ and Z^0. For example, the VX invariant mass distributions for spin 2 and a scalar 0^+ particle are very different, as seen in Fig. 13 [52], as also are the invariant mass distributions for a pseudoscalar 0^- particle. The Tevatron experiments have studied the related transverse-mass distribution, as seen in Fig. 14, and have found that the spin-2 and 0^- hypotheses are disfavoured at the 99% CL [53] - assuming that these experiments have indeed observed the same particle as discovered by ATLAS and CMS.

The differences in the couplings also lead to different energy dependences in the spin-2, 0^+ and 0^- cases, as seen in the left panel of Fig. 15. If one accepts the Tevatron evidence for $H(126)$ production, the ratio of the cross section to that at the LHC is also strong evidence against the spin-2 and 0^- hypotheses, as seen in the right panel of Fig. 15.

The polar angle distributions in the $H(126)$ centre-of-mass frame under the spin-2 and -0 hypotheses are also expected to be easily distinguishable. In the case of $gg \to H \to \gamma\gamma$ production, one

[5] Another problem for this scenario is that one expects, as in QCD, that the tensor boson should have a higher mass than the lightest Kaluza-Klein vector boson, which has not been seen.

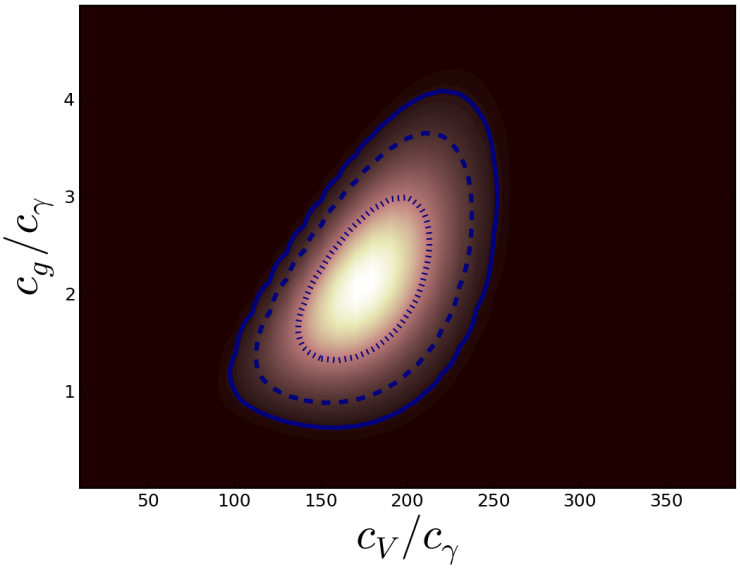

Fig. 12: The correlation between the values of c_W/c_γ (horizontal axis) and c_g/c_γ (vertical axis) found in a global fit to the current experimental data under the spin- two hypothesis [58].

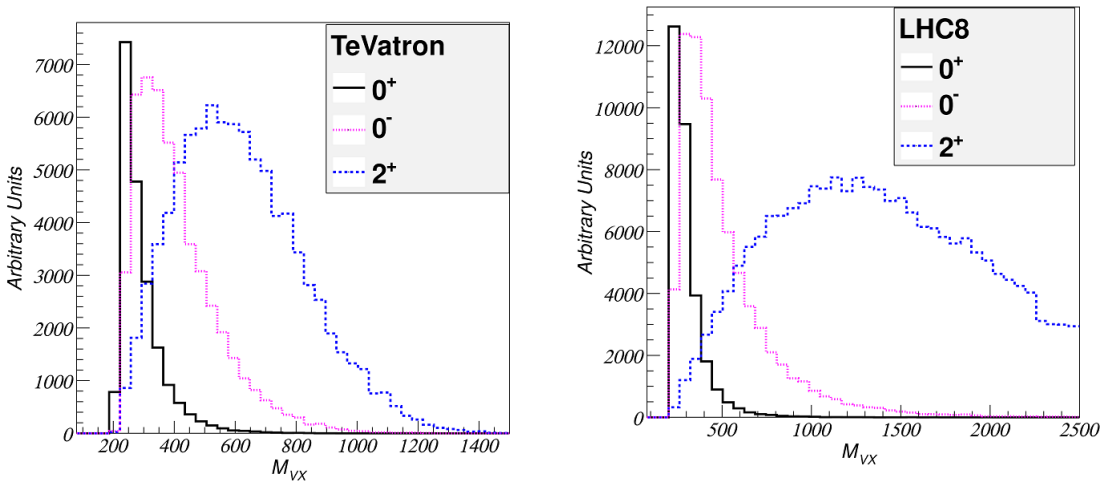

Fig. 13: The distributions in the $Z + H$ invariant mass M_{ZH} for the 0^+ (solid black), 0^- (pink dotted) and 2^+ (blue dashed) assignments for the H particle discovered by ATLAS [1] and CMS [2], calculated for the reaction $\bar{p}p \to Z + H$ at the TeVatron (left) and for the reaction $pp \to Z + H$ at the LHC at 8 TeV (right) [52].

expects the initial state to be an incoherent superposition of parallel and antiparallel gluon spins along the proton-proton collision axis. This knowledge of the initial state enables the final-state $\gamma\gamma$ polar-angle distribution to be calculated: it is expected to be non-uniform and peaked in the forward and backward directions, whereas the angular distribution would be isotropic in the spin-0 case. The ATLAS Collaboration has found that the spin-2 case is disfavoured at more than the 99% CL [59], and has extended the analysis to include an arbitrary admixture of $\bar{q}q$ initial states (which would be suppressed in the warped compactification scenario discussed above).

The azimuthal and polar angle distributions of the charged leptons in $H \to W^\pm W^{\mp *} \to \ell^+\ell^- + \ldots$ decays also provide significant power to distinguish between the spin-2 and -0 hypotheses [55, 57],

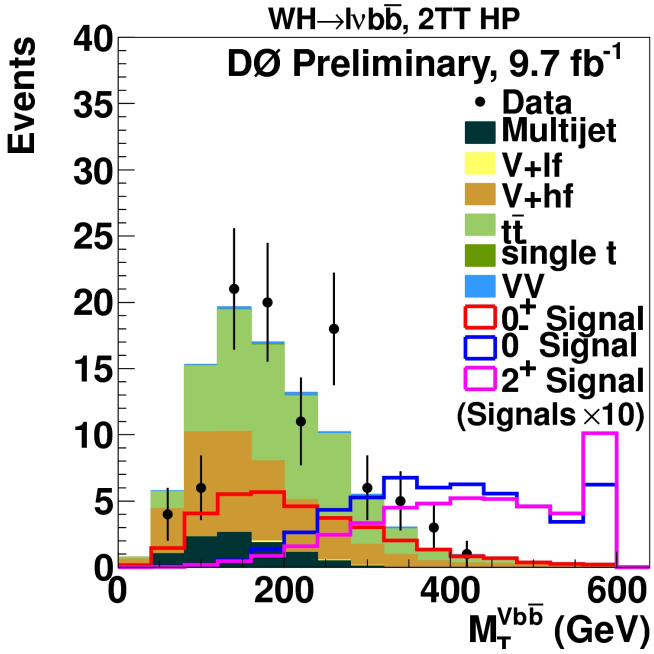

Fig. 14: The distribution in the $Z + H$ transverse mass M_{ZH} measured by the D0 Collaboration compared with simulations for the 0^+ (red), 0^- (blue) and 2^+ (mauve) hypotheses for the H particle [53].

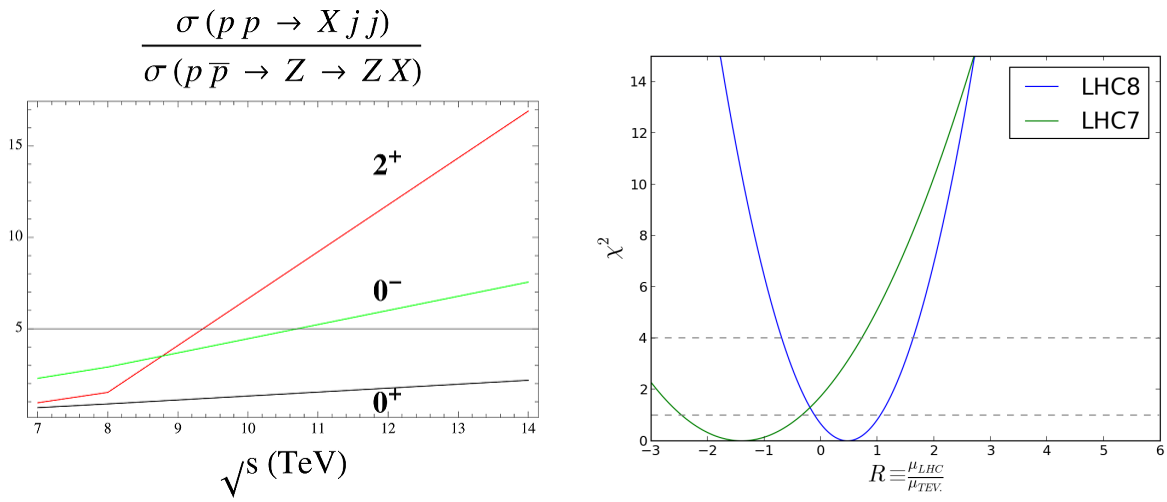

Fig. 15: Left - The energy dependence of the cross section for production of h in association with a Z boson under different hypotheses for the J^P of H: 0^+ (black), 2^+ (red) and 0^- (green). Right - The likelihood for the ratio $R_{\text{data}} = \mu_{\text{LHC 8}}/\mu_{\text{TeVatron}}$ extracted from the experimental data at 8 TeV (blue) and 7 TeV (green). The spin-two expectations $R_{\text{Spin 2}} = 5.4$ and 6.7 for 7 and 8 TeV, respectively, are excluded, and the 0^- expectations $R_{0^-} = 3.1$ and 2.7 for 7 and 8 TeV, respectively, are highly disfavoured, whereas the 0^+ expectation $R = 1$ is quite consistent with the data [54].

as seen in Fig. 16, and also disfavour the interpretation of $H(126)$ as a spin-2 particle with graviton-like couplings. Finally, the multiple kinematical observables in $H \to Z^0 Z^{0*} \to 2\ell^+ 2\ell^-$ also provide many powerful ways to distinguish between different spin-parity assignments for the $H(126)$ particle.

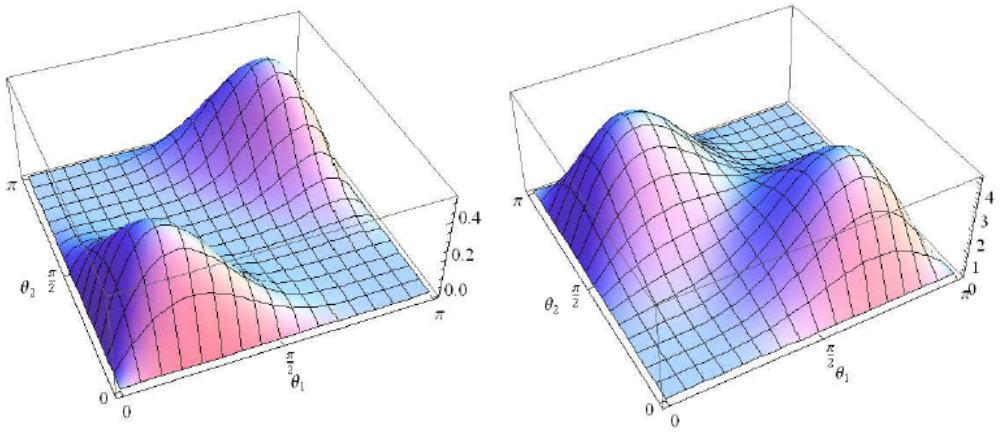

Fig. 16: Correlated distributions for the lepton polar angles in $H \to W^{\pm} W^{\mp *} \to \ell^+ \ell^- + \ldots$ decays for the 0^+ assignment (left panel) and for a graviton-like 2^+ particle (right panel) [55].

It is on the basis of a combination of $\gamma\gamma, W^{\pm} W^{\mp *}$ and $Z^0 Z^{0*}$ measurements, the ATLAS Collaboration has been able to exclude the graviton-like spin-2 hypothesis at more than the 99.9% CL, as seen in Fig. 17 [59]. Peter Higgs can continue smiling!

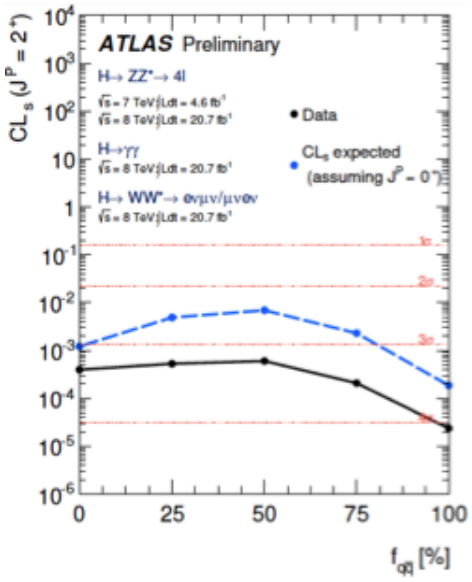

Fig. 17: Combining measurements in the $H \to \gamma\gamma, ZZ^* \to 4\ell^{\pm}$ and $WW^* \to 2\ell^{\pm}\nu\bar{\nu}$ final states, the ATLAS Collaboration excludes the spin-2 hypothesis for H at more than the 99.9% CL for any combination of H production via gg and $\bar{q}q$ collisions [59].

2.2.2 Is it Scalar or Pseudoscalar?

As has been discussed above, many of the analyses that discriminate between the spin-2 and 0^+ hypotheses can also be used to discriminate between 0^- and 0^+. For example, the $V + H$ invariant mass distributions in associated production are different, and already disfavour 0^- quite strongly. The angu-

lar distribution of the $\gamma\gamma$ final state does not distinguish, but the angular and kinematic distributions in $H \to W^{\pm}W^{\mp *} \to \ell^+\ell^- + \ldots$ and $H \to Z^0Z^{0*} \to 2\ell^+2\ell^-$ do offer discrimination between 0^+ and 0^- [57]. Thus the possibility of a pure 0^- spin-parity assignment can also be excluded beyond the 99% CL [59].

On the other hand, in the presence of CP violation the H particle could decay as a mixture of scalar and pseudoscalar, and the fractions could be different in different final states. At the moment, the admixture of a substantial fraction of pseudoscalar final states in $H \to W^{\pm}W^{\mp *}$ and $H \to Z^0Z^{0*}$ decays cannot be excluded. It is important to extend probes of a possible 0^- admixture to final states involving fermions, and measurements in $\tau^+\tau^-$ final states, $\bar{t}t + H$ and single $t + H$ production (see later) have been proposed [44]. But, for the time being, Peter Higgs can continue smiling!

2.2.3 Is it Elementary or Composite?

This question may be addressed by constructing a phenomenological Lagrangian $\mathcal{L}$ with free parameters to describe the interactions of the 'Higgs' boson, and constraining the parameters using data on H production and decay. Motivated by the success of the Standard Model relation $\rho \equiv m_W/m_Z \cos\theta_W = 1$, it is usually assumed that this phenomenological Lagrangian possesses a custodial symmetry: SU(2)×SU(2) → SU(2). In this case, one may parameterize the leading-order terms in $\mathcal{L}$ as follows [60]:

$$\begin{aligned}
\mathcal{L} &= \frac{v^2}{4}\mathrm{Tr}D_\mu\Sigma^\dagger D^\mu\Sigma\left(1 + 2a\frac{H}{v} + b\frac{H^2}{v^2} + \ldots\right) \\
&- \bar{\psi}^i_L\Sigma\left(1 + c\frac{H}{v} + \ldots\right) \\
&+ \frac{1}{2}\left(\partial_\mu H\right)^2 + \frac{1}{2}m_H^2H^2 + d_3\frac{1}{6}\left(\frac{3m_H^2}{v}\right)H^3 + d_4\frac{1}{24}\left(\frac{3m_H^2}{v}\right)H^4 + \ldots\,,
\end{aligned} \tag{73}$$

where

$$\Sigma \equiv \exp\left(i\frac{\sigma^a\pi^a}{v}\right)\,, \tag{74}$$

and the effective interaction with massless gauge bosons is written as

$$\mathcal{L}_\Delta = -\left(\frac{\alpha_s}{8\pi}c_g G_{a\mu\nu}G_a^{\mu\nu} + \frac{\alpha_{em}}{8\pi}c_\gamma F_{\mu\nu}F^{\mu\nu}\right)\left(\frac{H}{v}\right)^2\,. \tag{75}$$

The free coefficients a, b, c, d_3, d_4, c_g and c_γ are all normalized such that they are unity in the Standard Model: composite models may give observable deviations from these values. For example, in the composite model known as MCHM4 one has [51]

$$a = c = \sqrt{1-\xi} \,:\, \xi \equiv \left(\frac{v}{f}\right)^2\,, \tag{76}$$

where f is an analogue of the pion decay constant in QCD. On the other hand, in the MCHM5 composite model, one has

$$a = \sqrt{1-\xi}\,,\; c = \frac{1-2\xi}{\sqrt{1-\xi}}\,, \tag{77}$$

and in a pseudo-dilaton model one has

$$a = c = \frac{v}{V}\,, \tag{78}$$

where V is the dilaton v.e.v. that breaks scale invariance. On may also consider an 'anti-dilaton' scenario in which $a = -c$.

The signal strengths R in various channels relative to the Standard Model values are related in an obvious way to the parameters in (73). For example, for vector boson fusion and production in association with $V = W, Z$ one has

$$R_{VBF} \; = \; R_{VH} \; = \; a^2 \, , \tag{79}$$

and for production in association with $\bar{t}t$ and the rates for decays into $\bar{b}b$ and $\tau^+\tau^-$ one has

$$R_{\bar{f}f} \; = \; c^2 \, . \tag{80}$$

The corresponding ratio for the ggH coupling strength depends on the $\bar{t}t$ coupling:

$$R_{gg} \; = \; c_g^2 \; = \; c^2 + \ldots \, , \tag{81}$$

where the $\ldots$ represent possible contributions from particles beyond the Standard Model, and the ratio for the $H\gamma\gamma$ coupling depends on both a and c as well as possible non-Standard Model contributions:

$$R_{\gamma\gamma} \; = \; c_\gamma^2 \; = \; \frac{\left(-\frac{8}{3} c F_t + a F_W\right)^2}{\left(-\frac{8}{3} F_t + F_W\right)^2} + \ldots \, , \tag{82}$$

where $F_{t,W}$ are form factors that depend on the ratios m_H/m_t and m_H/m_W, respectively. It is apparent from these expressions that only $R_{\gamma\gamma}$ is sensitive to the relative sign of the $H\bar{f}f$ and HVV couplings. The principal dependences of the signal strengths in various channels on the a and c parameters in (73) are summarized in Table 2.

	Production sensitive to		Decay sensitive to	
channel	a	c	a	c
$\gamma\gamma$	✓	✓	✓	✓
$\gamma\gamma$ VBF	✓	×	✓	✓
WW	✓	✓	✓	×
WW + 2 jets	✓	×	✓	×
WW + 0,1 jet	×	✓	✓	×
$b\bar{b}$	✓	×	×	✓
ZZ	✓	✓	✓	×
$\tau\tau$	✓	✓	×	✓
$\tau\tau$ VBF, VH	✓	×	×	✓

Table 2: The dominant dependences on the model parameters (a, c) (73) of the H signal strengths in various channels, from [61].

Fig. 18 shows how measurements of these various channels at the Tevatron collider and the LHC combine to constrain the parameters (a, c) [51]. We see in the top left panel that the data on $\bar{b}b$ final states already disfavour leptophobic models in which the H particle has no couplings to fermions - here the Tevatron experiments play an important rôle. In the top right panel we see that data on the $\tau^+\tau^-$ final state also disfavour leptophobic models. However, as expected on the basis of (80), these measurements by themselves offer no information about the sign of the fermion coupling coefficient c. The middle left panel shows the constraint imposed by the data on the $\gamma\gamma$ final state. As seen in (82), this final state gives a constraint that is not symmetric between the signs of c, since there is interference between the virtual $\bar{t}t$ and W^+W^- intermediate states that may be either constructive of destructive, depending on the sign of c. The middle right panel of Fig. 18 shows the constraint imposed by measurements of WW^* final states as well as H production via W^+W^- VBF and production in association with $W^\pm$, and the bottom left panel shows the corresponding constraint on the HZZ coupling. These measurements are highly consistent with custodial symmetry: SU(2)×SU(2) → SU(2), as assumed in writing (73).

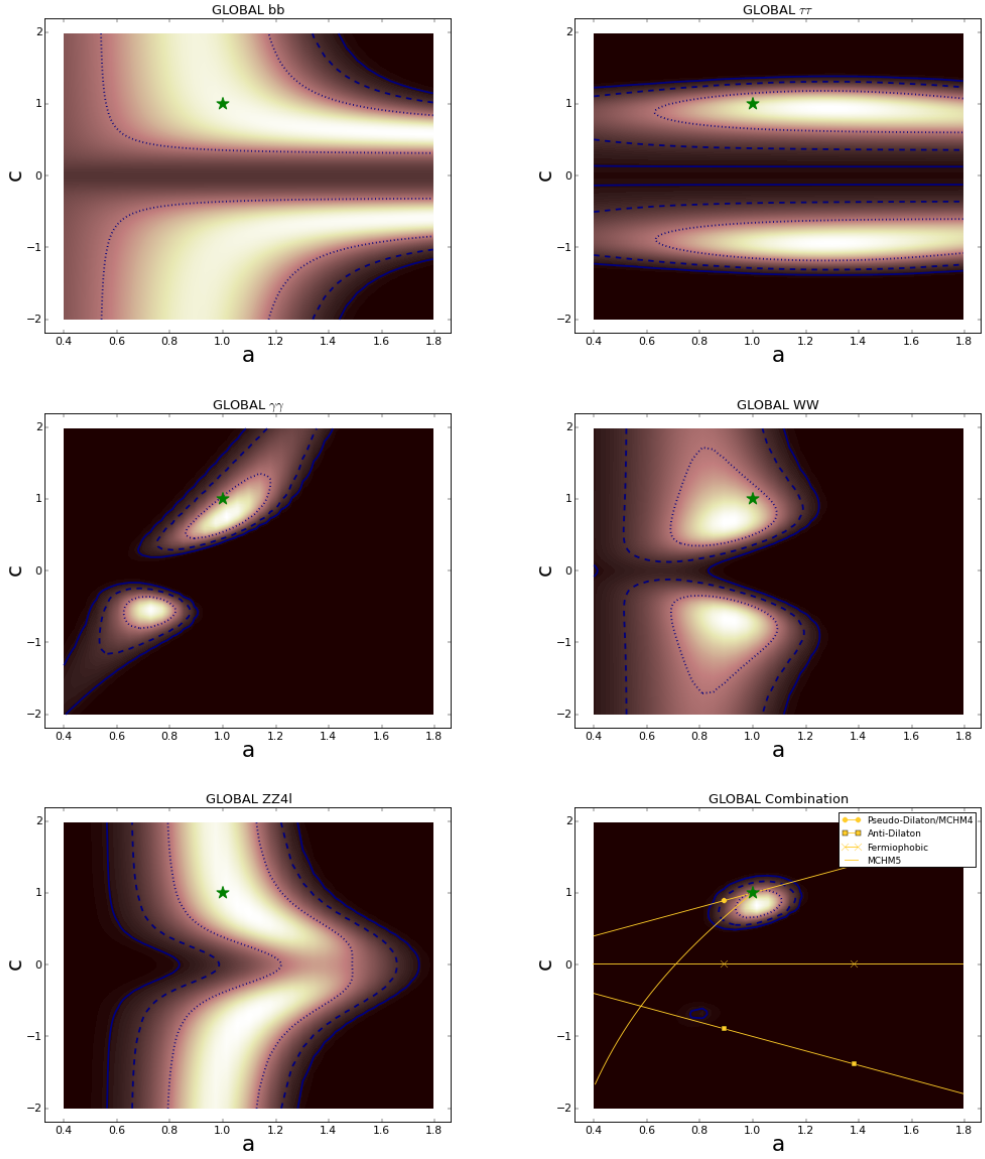

Fig. 18: The constraints in the (a, c) plane imposed by the measurements in Fig. 11 of the $\bar{b}b$ final state (top left), of the $\tau^+\tau^-$ final state (top right), of the $\gamma\gamma$ final state (middle left), of the WW coupling (middle right) and in the ZZ coupling (bottom left). The combination of all these constraints is shown in the bottom right panel [51].

Finally, the bottom right panel of Fig. 18 displays the constraints in the (a, c) plane obtained in a global combination of these measurements [51]. We see that the positive sign of c, as expected in the Standard Model, is strongly favoured. This point is made explicitly in Fig. 19, where we see that the data favour $a \sim 1$ and disfavour $c < 0$ by $\Delta\chi^2 \sim 9$, i.e., 3 standard deviations. The continuous yellow lines the bottom right panel of Fig. 18 show the predictions of various composite alternatives to the Standard Model. As already mentioned, leptophilic models (represented by the horizontal line) are strongly disfavoured, as are 'anti-dilaton' models with $a = -c$ (downwards-sloping line). The global analysis is compatible with the MCHM4 and dilaton models *iff* they are tuned to resemble the Standard Model, with $\xi \sim 0, f \sim v$ in the MCHM4 (76) or $V \sim v$ in the pseudo-dilaton (78) model (upwards-sloping line). Likewise, the MCHM5 model is compatible with the data only if $\xi \sim 0$ in (77). Clearly, there is no evidence for any significant deviation from the Standard Model, and Peter Higgs may continue to smile!

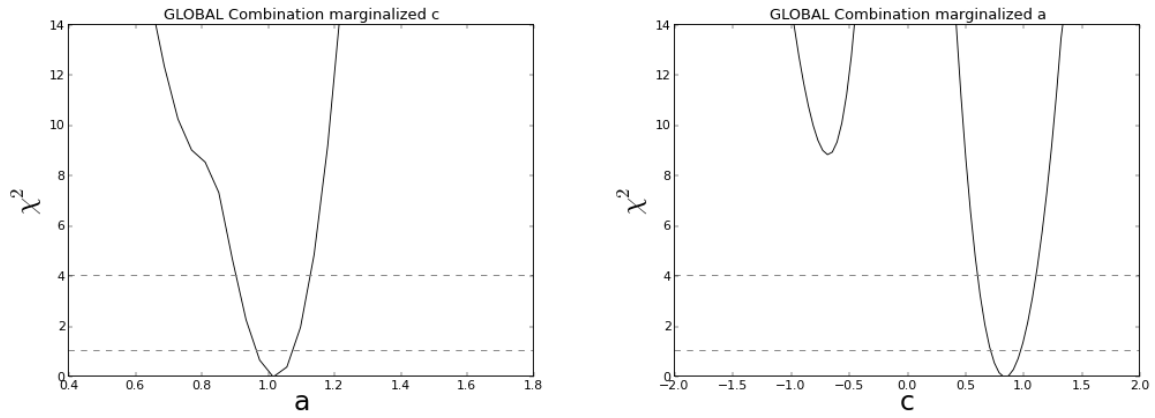

Fig. 19: The one-dimensional likelihood functions for the boson coupling parameter a (left panel) and the fermion coupling parameter c (right panel), as obtained by marginalizing over the other parameter in the bottom right panel of Fig. 18 [51].

Before concluding this Section, it is interesting to discuss in more detail a Higgs production channel that could give direct information on the sign and magnitude of c, namely single t (or $\bar{t}$) production in association with H [42,43]. The two dominant amplitudes are due to Higgsstrahlung from an exchanged W boson and the final-state t quark. In the Standard Model with $c > 0$, these diagrams interfere destructively, as a precursor of the good high-energy behaviour expected in a spontaneously-broken gauge theory, whereas if $c < 0$ the production cross section may be much larger. Even establishing an upper limit on single t (or $\bar{t}$) production in association with H may be sufficient to determine the sign of c, independently of the $\gamma\gamma$ measurement [43]. One may also consider the possibility of a CP-violating $\bar{t}tH$ vertex $\tilde{c}_t$ in addition to a conventional scalar vertex with coefficient c_t relative to the Standard Model value. The right panel of Fig. 20 shows the dependences of the $\bar{t}tH$, tH and $\bar{t}H$ cross sections on $\zeta_t \equiv \arctan(\tilde{c}_t/c_t)$ [44] for choices of the c_t and $\tilde{c}_t$ that are compatible with the constraints on the Hgg and $H\gamma\gamma$ couplings shown in Fig. 23 [51]. We see that measurements of the $\bar{t}tH$, tH and $\bar{t}H$ cross sections could provide interesting information on the top-H couplings.

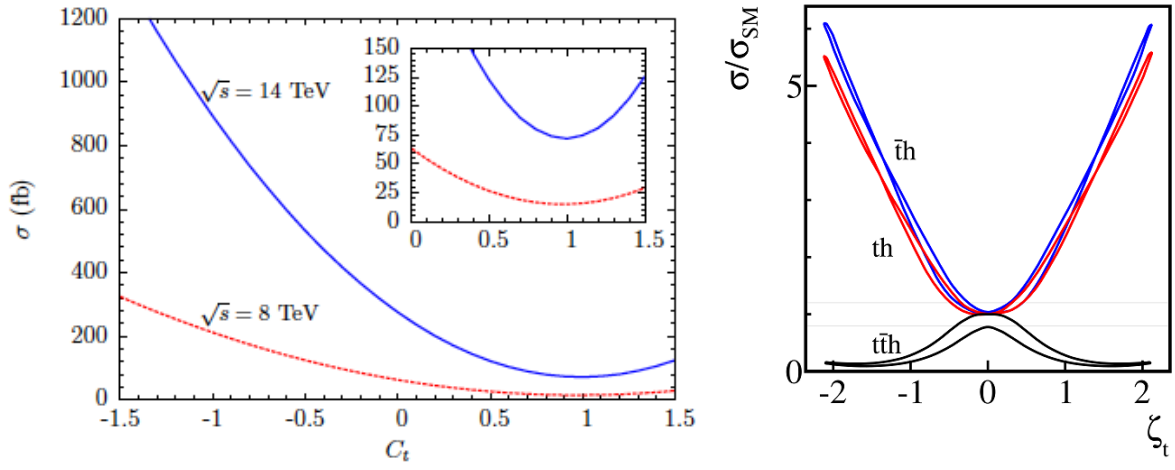

Fig. 20: Left panel: The cross section for single $t + H$ production as a function of the scalar top-H coupling c_t normalized to its Standard Model value [43]. Right panel: The cross sections for $\bar{t}t + H$, single t and $\bar{t} + H$ production relative to their Standard Model values for ranges of the scalar and pseudoscalar couplings $(c_t, \tilde{c}_t)$ compatible with current data on $gg \to H$ production and $H \to \gamma\gamma$ decay [51], as functions of $\zeta_t \equiv \text{arc}\tan(c_t/\tilde{c}_t)$ [44].

2.2.4 *Are its Couplings Proportional to Particle Masses?*

It is a key property of the Higgs boson of the Standard Model that its couplings to other particles should be proportional to their masses, and this is verified implicitly by the type of analysis reviewed in the previous Section. In order to verify it more explicitly, we may consider a parametrization of the H couplings to fermions λ_f and massive bosons g_V of the form [51, 61]

$$\lambda_f \; = \; \sqrt{2} \left(\frac{m_f}{M} \right)^{1+\epsilon} , \; g_V \; = \; 2 \left(\frac{m_V^{2(1+\epsilon)}}{M^{1+2\epsilon}} \right) . \tag{83}$$

In the Standard Model, one would expect the power $\epsilon = 0$ and the scaling coefficient $M = v = 246$ GeV. The results of a fit in terms of the two parameters (M, ϵ) is shown in Fig. 21. It is represented in the left panel by the dashed line, with the one-σ excursions shown as dotted lines. The solid red line is the prediction of the Standard Model, and the points with error bars are the predictions of the two-parameter fit. We see that these are completely compatible with the Standard Model predictions. In the right panel of Fig. 21 we see the 68 and 95% CL regions given by the fit in the (M, ϵ) plane. Here the solid horizontal and vertical lines represent the Standard Model predictions $\epsilon = 0$ and $M = 246$ GeV. The data are quite close to the bull's eye! We display in the left panel of Fig. 22 the one-dimensional χ^2 function for ϵ, marginalized over M, and in the right panel the one-dimensional χ^2 function for M, marginalized over ϵ. The central values and the 68% CL ranges of M and ϵ are:

$$M \; = \; 244^{+20}_{-10} \; \text{GeV} \; , \; \epsilon \; = \; -0.022^{+0.042}_{-0.021} \, . \tag{84}$$

As we wrote in [61]: *"It walks and quacks like a Higgs boson."*

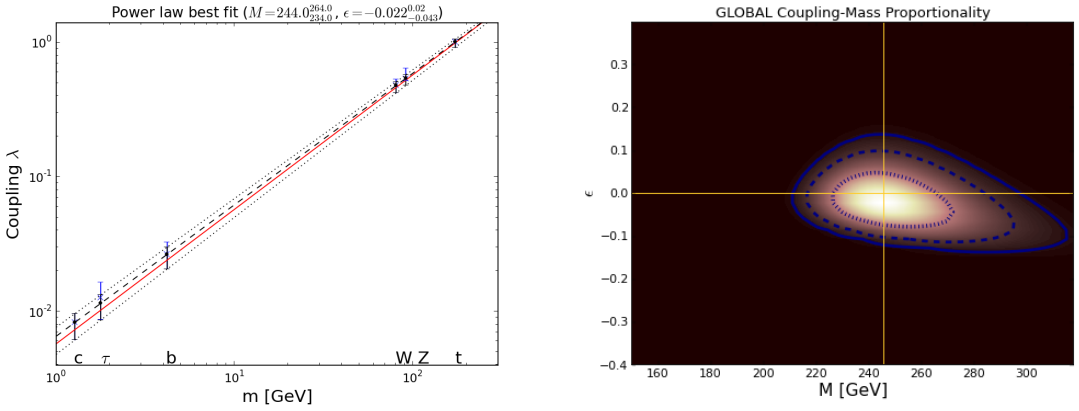

Fig. 21: The constraints on M and ϵ (83) imposed by the measurements in Fig. 11. The left panel shows the strengths of the couplings to different fermion flavours and massive bosons predicted by this two-parameter (M, ϵ) fit. The red line is the Standard Model prediction, the black dashed line is the best fit, and the dotted lines are the 68% CL ranges. For each particle species, the black error bar shows the range predicted by the global fit, and the blue error bar shows the range predicted for that coupling if its measurement is omitted from the global fit. The right panel displays the fit constraint in the (M, ϵ) plane [51].

2.2.5 *Are there Extra Contributions to its Loop Couplings?*

The previous two Sections show that the tree-level H couplings are similar to those of a Standard Model Higgs boson. What can one say about its loop couplings to gg and $\gamma\gamma$? Here we assume that its couplings to fermions and massive vector bosons are indeed Standard Model-like, so that $a = c = 1$, and investigate whether there is any evidence for other coloured (in the case of the gg coupling) or charged (in the case

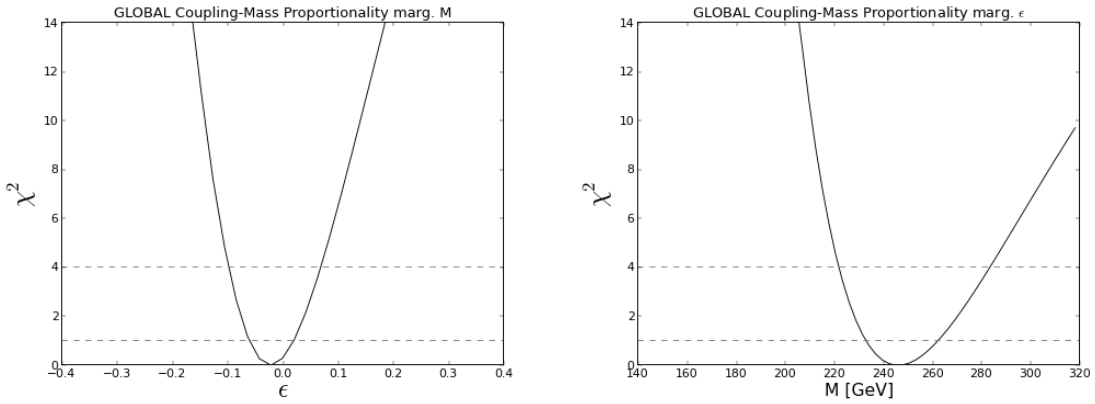

Fig. 22: The one-dimensional χ^2 functions for ϵ (left panel) and M (right panel), as obtained by marginalizing over the other fit parameter [51].

of the $\gamma\gamma$ coupling) particles contributing via triangular loop diagrams, so that c_g and/or $c_\gamma \neq 1$ in (75). We see in Fig. 23 that the central value of $c_\gamma > 1$ and the central value of $c_g < 1$ [51]:

$$c_\gamma \; = \; 1.18 \pm 0.12 \; , \; c_g \; = \; 0.88 \pm 0.11 \; . \tag{85}$$

However, the data are compatible with the Standard Model at the 68% CL, as seen by the location of the green star in Fig. 23. Thus, there is no good evidence for new particles circulating in loop diagrams. Fig. 24 displays the one-dimensional χ^2 functions for c_γ (left panel) and c_g (right panel), assuming, as above that $a = c = 1$, so that the the tree-level couplings to massive bosons and fermions have the Standard Model values.

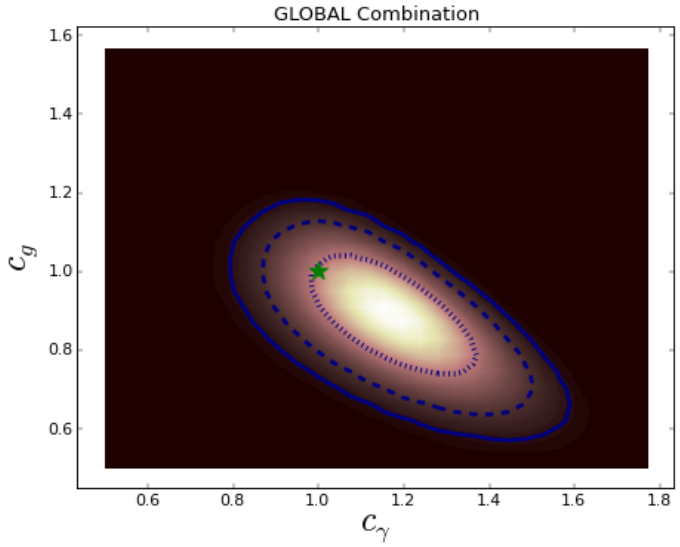

Fig. 23: The constraints in the (c_γ, c_g) plane imposed by the measurements in Fig. 11, assuming that $a = c = 1$, i.e., the Standard Model values for the tree-level couplings to massive bosons and fermions [51].

2.2.6 What is its Total Decay Rate?

We now assume that the Higgs has no other decays beyond those in the Standard Model, and discuss the total Higgs decay rate in the two global fits discussed above, in terms of the parameters (a, c) and (M, ϵ)

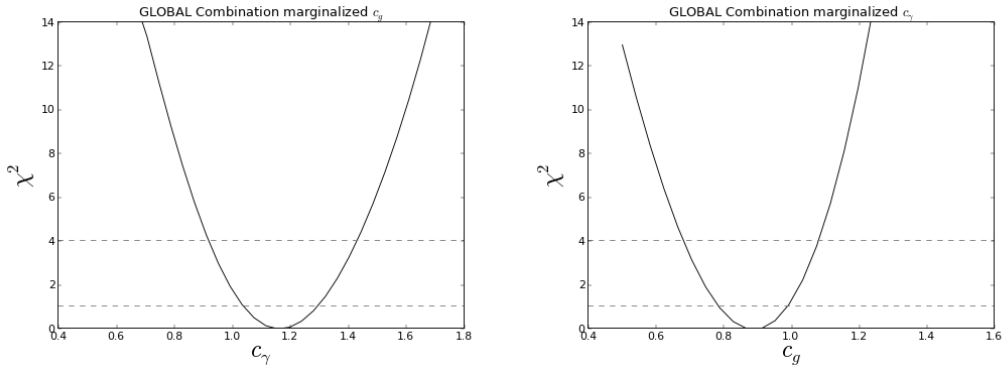

Fig. 24: The one-dimensional χ^2 functions for c_γ (left panel) and c_g (right panel), assuming that $a = c = 1$, so that the tree-level couplings to massive bosons and fermions have the Standard Model values [51].

and assuming no contributions from non-Standard-Model particles. The left panel of Fig. 25 displays contours of the Higgs decay width relative to the Standard Model prediction in the (a, c) plane shown in the bottom right panel of Fig. 18, and the right panel of Fig. 25 displays analogous contours in the (M, ϵ) plane. We see that in each case the best fit has a total decay rate close to the Standard Model value. Fig. 26 displays the one-dimensional χ^2 function for the total Higgs decay width relative to its Standard Model value. The solid line is obtained assuming that $a = c$ (or, equivalently, that $\epsilon = 0$ but M is free), the dashed line is obtained by marginalizing over (a, c), and the dot-dashed line is obtained by marginalizing over (M, ϵ). In all cases, we see that the total H decay width is compatible with the Standard Model prediction [51].

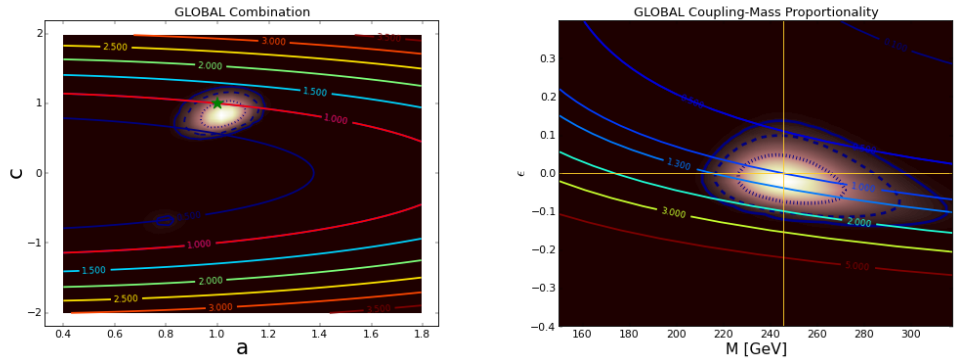

Fig. 25: Contours of the total Higgs decay rate relative to the Standard Model prediction in the (a, c) plane shown in the bottom right panel of Fig 18 (left) and the (M, ϵ) plane shown in the right panel of Fig. 21 (right) [51].

In the absence of an assumption about H decays into non-Standard Model particles, it is difficult to obtain an accurate measurement of the total Higgs decay rate Γ_H. The CMS Collaboration has given a model-independent upper limit of 3 GeV, based on the width of the $H \to \gamma\gamma$ signal peak that they observe, which is dominated by the experimental resolution. It has also been suggested [62] that one could establish an upper limit on Γ_H using measurements of ZZ final states mediated by off-shell H bosons. Using CMS data for $m_{ZZ} \in (100, 800)$ GeV, it was estimated in [62] that $\Gamma_H < 163$ MeV at the 95% CL, it was suggested that restricting to $M_{ZZ} > 300$ GeV this bound could be improved to $\Gamma_H < 88$ MeV, and it was suggested that the ultimate LHC sensitivity would be to $\Gamma_H \sim 40$ MeV (see also [63]). Similar sensitivity may be obtained from an analysis of off-resonance W^+W^- final states [64].

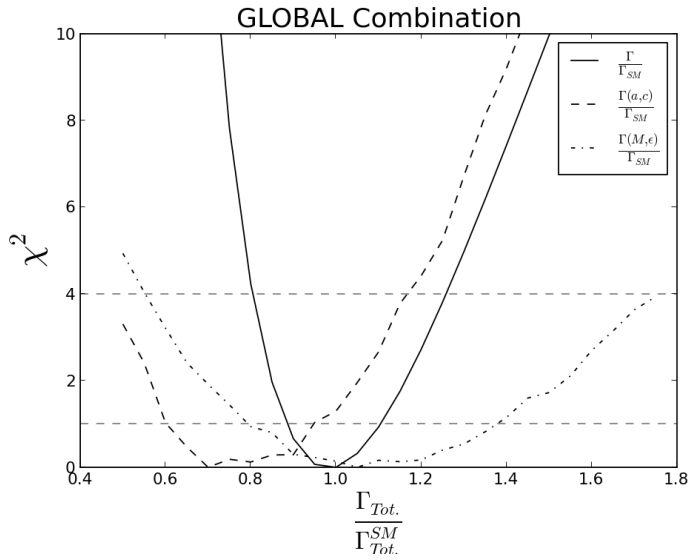

Fig. 26: The one-dimensional χ^2 function for the total Higgs decay width relative to its value in the Standard Model, $R \equiv \Gamma/\Gamma_{SM}$, assuming decays into Standard Model particles alone and assuming $a = c$ or equivalently $\epsilon = 0$ (solid line), marginalizing over (a, c) (dashed line) and marginalizing over (M, ϵ) (dot-dashed line) [51].

Another way to constrain or measure Γ_H may be via interference effects between the QCD and H contributions to the $\gamma\gamma$ final state, which could shift the $\gamma\gamma$ peak relative to its position in the $ZZ^* \to 4\ell^\pm$ final state. (These are the only two observed H states where the invariant mass can be measured accurately.) This mass shift is sensitive to the sign and magnitude of the $H\gamma\gamma$ coupling, by an amount that depends on the production kinematics. For Γ_H similar to the Standard Model value, the mass shift $\sim$ 70 MeV, as seen in Fig. 27 [65], so this is not a measurement for the faint-hearted! The published mass measurements have the problems that ATLAS and CMS find opposite signs for the $\gamma\gamma$ and $4\ell^\pm$ final states, though they are compatible within the experimental uncertainties, and their sensitivity is not yet very interesting.

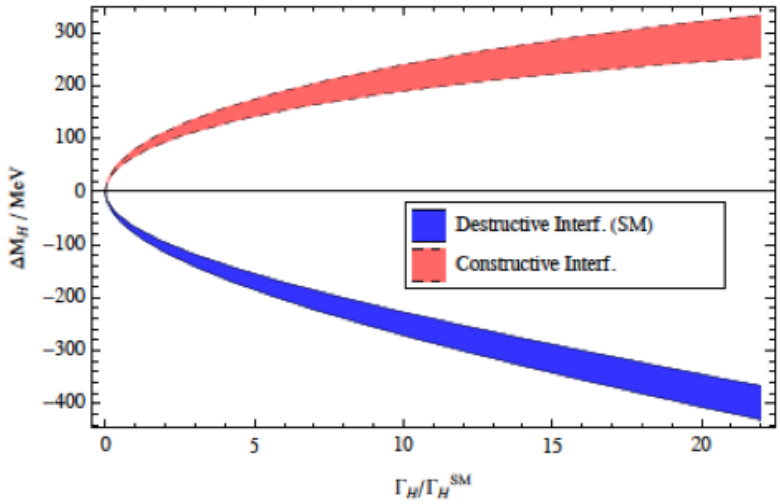

Fig. 27: The shift ΔM_H between measurements of the H mass in the $\gamma\gamma$ and $4\ell^\pm$ final states due to interference with QCD processes yielding $\gamma\gamma$ final states, calculated in NLO QCD as a function of Γ_H relative to its value in the Standard Model [65].

2.2.7 The Story so Far

The discovery of the H particle has opened a new chapter in particle physics. Alternatives to the expectation that it is a scalar boson have been excluded with a high degree of confidence, and its couplings are consistent with those of a Standard Model Higgs boson. In particular, they exhibit the expected correlation with the masses of other particles. This is why we wrote in [51]: *"Beyond any reasonable doubt, it is a Higgs boson."* [6].

Experiments are placing severe constraint on composite models, pushing upwards the possible scale of compositeness. On the other hand, an elementary scalar is a challenge for theorists, in particular because of the issue of quadratic divergences, that are symptomatic of extreme sensitivity to details of the ultraviolet completion. However, an elementary Higgs boson fits naturally within supersymmetry and, as we shall see in the next Section, simple supersymmetric models predict a Higgs mass below ~ 130 GeV, as observed, and also predict that its couplings should be very similar to those of a Standard Model Higgs boson. As yet, there are no signs of supersymmetric particles, and we wait with interest to see what the LHC will reveal at 13/14 TeV, and in its high-luminosity incarnation.

In 1982 I was introduced to Mrs. Thatcher when she visited CERN, and she asked me what I did. I replied that *"My job as a theorist is to think of thing for the experiments to look for, but then we hope they find something different."* Mrs. Thatcher liked things to be the way she wanted them to be, so she asked *"Wouldn't it be better if they found what you predicted?"*. I responded along the lines that *"If they just find exactly what we predict, we would have no clues how to progress."* In this spirt, let us all hope that the Higgs boson is not exactly that of the Standard Model, and that higher-energy LHC running will reveal other new physics beyond the Standard Model. In the next lecture I will discuss some of the prospects for these hopes.

3 What may the Future hold?

3.1 Theoretical Confusion

So far, though experiments at the LHC have discovered the Higgs boson, as yet they have found no direct hint of any new physics beyond the Standard Model such as supersymmetry or compositeness. The combination of these facts has caused a high mortality rate among theories, though not among theorists! As discussed previously, however, the fact that the measured values of m_H and m_t lie in a region where the electroweak vacuum would be unstable (OK, metastable) has led to suggestions that there should be new physics below 10^{10} GeV to stabilize the vacuum. There have also been suggestions that the proximity of (m_H, m_t) to the stability boundary may be an indirect hint for some new physical principle [7].

Supersymmetrists are among the most confused theorists. Motivated by the apparent fine-tuning of the electroweak scale and several phenomenological considerations such as dark matter, many of them had expected supersymmetry to appear during the first LHC run. In my view, this should be understood as the first run of the LHC at or close to its design energy of 14 TeV, so we should wait a while before jumping to conclusions. However, voices have been heard favouring very high-scale supersymmetry or split supersymmetry. The faint-hearted are asking whether we should modify or abandon the principle of naturalness. It is a reasonable question whether Nature needs to care about the naturalness of the electroweak scale, as long as she can find one set of parameters that includes the Standard Model. This is one possibility opened up by the string landscape, which comprises an exceedingly large number of possible vacua that all seem consistent with our current understanding. My own point of view is that supersymmetry anywhere would be better than nowhere, in terms of reducing the required amount of

[6] This phrase was quoted by the Royal Swedish Academy of Sciences in the Advanced Information it released about the award of the 2013 Nobel Physics Prize [66]. Ironically, this phrase had been removed from the published version of [51] at the request of the referee, who found the phrase *"unscientific"*.

[7] This is also sometimes linked to the fact that the cosmological constant (dark energy) lies close to the upper bound proposed by Weinberg [67].

fine-tuning. In any case, supersymmetry alone could not explain the hierarchy between the electroweak and gravitational scales: another mechanism would be needed to establish the hierarchy. New ideas are clearly needed!

In the absence of signatures of physics beyond the Standard Model at the LHC, there has been a tendency among some physicists to wonder whether the Standard Model is all there is, despite the persistence of a few loose ends such as the hierarchy, dark matter, the origin of matter, quantum gravity, etc. History gives many examples where such pessimism has turned out to be unwarranted: consider the examples of Albert Michelson (1894) *"The more important fundamental laws and facts of physical science have all been discovered"* or Lord Kelvin (1900) *"There is nothing new to be discovered in physics now. All that remains is more and more precise measurement"*, not to mention a Spanish Royal Commission, rejecting the proposal of Christopher Columbus to sail west (before 1492) *"So many centuries after the Creation, it is unlikely that anyone could find hitherto unknown lands of any value"*.

Perhaps we should rather follow the approach of Sherlock Holmes in the "Silver Blaze" story who, when asked by a policeman *"Is there any other point to which you would wish to draw my attention?"*, responded *"To the curious incident of the dog in the night-time."* The policeman then remarked that *"The dog did nothing in the night-time"*, to which Holmes replied *"That was the curious incident."* In our case, the *"curious incident"* is that no beyond the Standard Model dog has yet barked. Nevertheless, experiments have already provided theorists with many other clues: perhaps we need next to examine them more carefully, as well as planning ambitious future experiments. These are the themes of this Lecture.

3.2 Additional Topics in Higgs Studies

3.2.1 Higher-Dimensional Operators

A powerful way to probe indirectly possible physics beyond the Standard Model is to consider additional higher-dimensional operators that might be generated by new physics such as the exchanges of heavy particles, use data to constrain their coefficients, and thereby constrain the possibilities for physics beyond the Standard Model. In principle, this offers a way to constrain new physics in a coherent and effective way using a formalism that is consistent with all the established gauge and other symmetries. As an example, the CP-conserving dimension-6 operators in an effective Lagrangian involving just boson fields may be written in the form [68]:

$$\mathcal{L}_{CP+6} = \frac{\bar{c}_H}{2v^2}\partial^\mu\left[\Phi^\dagger\Phi\right]\partial_\mu\left[\Phi^\dagger\Phi\right] + \frac{\bar{c}_T}{2v^2}\left[\Phi^\dagger\overleftrightarrow{D}^\mu\Phi\right]\left[\Phi^\dagger\overleftrightarrow{D}_\mu\Phi\right] - \frac{\bar{c}_6\lambda}{v^2}\left[H^\dagger H\right]^3 \quad (86)$$

$$+ \frac{ig\,\bar{c}_W}{m_W^2}\left[\Phi^\dagger T_{2k}\overleftrightarrow{D}^\mu\Phi\right]D^\nu W^k_{\mu\nu} + \frac{ig'\,\bar{c}_B}{2m_W^2}\left[\Phi^\dagger\overleftrightarrow{D}^\mu\Phi\right]\partial^\nu B_{\mu\nu} \quad (87)$$

$$+ \frac{2ig\,\bar{c}_{HW}}{m_W^2}\left[D^\mu\Phi^\dagger T_{2k}D^\nu\Phi\right]W^k_{\mu\nu} + \frac{ig'\,\bar{c}_{HB}}{m_W^2}\left[D^\mu\Phi^\dagger D^\nu\Phi\right]B_{\mu\nu} \quad (88)$$

$$+ \frac{g'^2\,\bar{c}_\gamma}{m_W^2}\Phi^\dagger\Phi B_{\mu\nu}B^{\mu\nu} + \frac{g_s^2\,\bar{c}_g}{m_W^2}\Phi^\dagger\Phi G^a_{\mu\nu}G_a^{\mu\nu}\,. \quad (89)$$

The coefficients $\bar{c}_H, \bar{c}_T, \bar{c}_W, \bar{c}_B, \bar{c}_{HW}, \bar{c}_{HB}, \bar{c}_\gamma$ and $\bar{c}_g$ may then be constrained using precision electroweak data, measurements of Higgs production and decays, triple-gauge-boson couplings, etc. These constraints may then be compared with calculations in specific extensions of the Standard Model such as supersymmetry or composite models. One can also consider a CP-violating set of dimension-6 bosonic operators:

$$\mathcal{L}_{CP-6} = \frac{ig\,\tilde{c}_{HW}}{m_W^2}D^\mu\Phi^\dagger T_{2k}D^\nu\Phi\widetilde{W}^k_{\mu\nu} + \frac{ig'\,\tilde{c}_{HB}}{m_W^2}D^\mu\Phi^\dagger D^\nu\Phi\widetilde{B}_{\mu\nu} + \frac{g'^2\,\tilde{c}_\gamma}{m_W^2}\Phi^\dagger\Phi B_{\mu\nu}\widetilde{B}^{\mu\nu} \quad (90)$$

$$+ \frac{g_s^2\,\tilde{c}_g}{m_W^2}\Phi^\dagger\Phi G^a_{\mu\nu}\widetilde{G}_a^{\mu\nu} + \frac{g^3\,\tilde{c}_{3W}}{m_W^2}\epsilon_{ijk}W^i_{\mu\nu}W^{\nu j}_{\ \ \rho}\widetilde{W}^{\rho\mu k} + \frac{g_s^3\,\tilde{c}_{3G}}{m_W^2}f_{abc}G^a_{\mu\nu}G^{\nu b}_{\ \ \rho}\widetilde{G}^{\rho\mu c}\,, \quad (91)$$

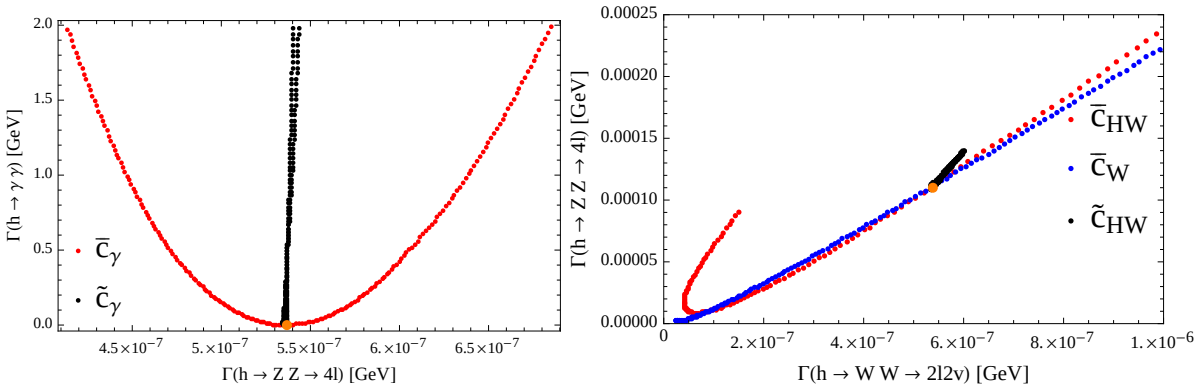

Fig. 28: Effects of the dimension-6 operators $\bar{c}_\gamma, \tilde{c}_\gamma, \bar{c}_{HW}, \bar{c}_W$ and $\tilde{c}_{HW}$ from (89, 90) on the $H \to ZZ^*$ and $\gamma\gamma$ partial widths (left panel) and the $H \to WW^*$ and $H \to ZZ^*$ partial widths (right panel). In each case, the Standard Model prediction is indicated by an orange dot [68].

where the dual field strength tensors are defined by

$$\widetilde{B}_{\mu\nu} = \frac{1}{2}\epsilon_{\mu\nu\rho\sigma}B^{\rho\sigma} \ , \quad \widetilde{W}^k_{\mu\nu} = \frac{1}{2}\epsilon_{\mu\nu\rho\sigma}W^{\rho\sigma k} \ , \quad \widetilde{G}^a_{\mu\nu} = \frac{1}{2}\epsilon_{\mu\nu\rho\sigma}G^{\rho\sigma a} \ . \tag{92}$$

Two specific examples of possible effects on H decays due to higher-dimensional operators are shown in Fig. 28. In the left panel, we see the effects of the terms $\propto \bar{c}_\gamma$ and $\tilde{c}_\gamma$ on $H \to ZZ^*$ and $\gamma\gamma$ decays, and in the right panel we the effects of the $\propto \bar{c}_{HW}, \bar{c}_W$ and $\tilde{c}_{HW}$ on $H \to ZZ^*$ and WW^* decays,.

Some of the operators in (89) and (90) may also affect the production cross sections and kinematic distributions of the H boson. An example is provided by the double ratio of the cross sections for H production in association with a vector boson at 14 and 8 TeV:

$$\mathcal{R} \ \equiv \ \left(\frac{\sigma(\sqrt{S} = 14 \text{ TeV})}{\sigma(\sqrt{S} = 8 \text{ TeV})}\right)_{\bar{c}_i} \Big/ \left(\frac{\sigma(\sqrt{S} = 14 \text{ TeV})}{\sigma(\sqrt{S} = 8 \text{ TeV})}\right)_{SM} \tag{93}$$

in the presence of an operator with coefficient $\bar{c}_i$, as illustrated in the left panel of Fig. 29 for the case of $\bar{c}_{HW}$. The right panel of Fig. 29 illustrates the effects on the WH invariant mass distribution for the cases $\bar{c}_{HW}$ (blue dotted histogram) and $\bar{c}_W = 0.1$ (black histogram), the shaded histogram being the prediction of the Standard Model. We see that the double ratio (93) and the invariant mass distribution are interesting tools for constraining such operator coefficients, just as they provide discrimination between the $0^+, 0^-$ and 2^+ hypotheses for the H spin.

3.2.2 A or The?

Now that the H particle has been established 'beyond any reasonable doubt" to be *a* Higgs boson, the questions arise whether it is *the* Higgs boson of the Standard Model, and whether there are any others. Possibilities proposed include models with an extra singlet field, models with a fermiophobic Higgs boson, and models with two Higgs doublets (2HDM) such as the minimal supersymmetric extension of the Standard Model (the MSSM). The ATLAS and CMS experiments have established upper limits on the couplings of possible massive H' boson, as we shall see later in connection with the MSSM.

Also on the agenda of the LHC experiments is to measure VV scattering and make a closure test, so as to check the Standard Model H cancellation discussed earlier. Does the Higgs boson discovered by ATLAS and CMS cure its high-energy behaviour so that the theory is indeed renormalizable?

Another strategy is to search for non-Standard Model decays, e.g., into invisible final states, or into pairs of light (pseudo)scalars aa, or into lepton-flavour-violating final states such as $\mu\tau$ or $e\tau$, as discussed in the next Section.

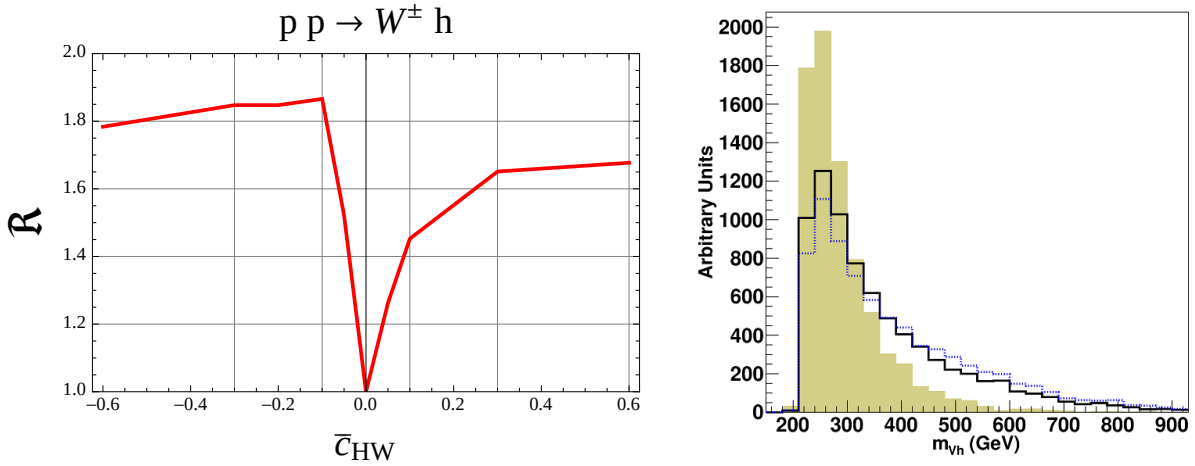

Fig. 29: Left panel: the double ratio $\mathcal{R}$ (93) of total cross sections at $\sqrt{S} = 8$ TeV and 14 TeV for the associated production process $pp \to W^{\pm}H \to \ell\nu b\bar{b}$ may provide a useful constraint on the dimension-6 operator coefficient $\bar{c}_{HW}$. Right panel: the invariant-mass distribution m_{VH} is displayed for the Standard Model (shaded histogram) and with additional couplings $\bar{c}_{HW} = 0.1$ (blue-dotted histogram) and $\bar{c}_W = 0.1$ (black histogram) [68].

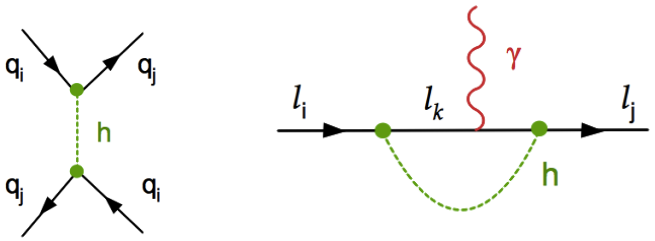

Fig. 30: Left: Tree-level diagram contributing to a generic flavour-changing amplitude via H exchange. Right: One-loop H loop diagram contributing to anomalous magnetic moments and electric dipole moments of charged leptons ($i = j$), or radiative LFV decay modes ($i \neq j$) [48].

3.2.3 Flavour-Changing H Decays

In the Standard Model one expects flavour-changing Higgs decays to occur only far below the sensitivity of present and prospective LHC measurements. However, this might not be true, e.g., in some composite Higgs models, so searches for flavour-violating H decays present an interesting opportunity to look for new physics beyond the Standard Model. Model-independent constraints on such decays are provided by measurements of flavour-violating processes at low energies, including the effects of four-fermion interactions generated by H exchange and H loop contributions to dipole moments, as illustrated in Fig. 30 [48].

Constraints from $\Delta F = 2$ processes such as $K - \bar{K}$, $D - \bar{D}$, $B - \bar{B}$ and $B_s - \bar{B}_s$ mixing constrain flavour-changing H couplings so severely that quark-flavour-violating H decays are too suppressed to be detectable in the foreseeable future. However, the upper limits on lepton-flavour-changing H couplings are much weaker, and leave open the possibility that either $H \to \tau\mu$ or $H \to \tau e$ might have a branching ratio as large as $\sim 10\%$, comparable to the branching ratio for $H \to \tau\tau$. (The upper limit on $\mu \to e\gamma$ forbids both branching ratios from being large simultaneously.) On the other hand, the constraints on the flavour-violating $H\mu e$ coupling from anomalous $\mu \to e$ conversion on nuclei and $\mu \to e\gamma$ are much stronger, and require $\mathrm{BR}(H \to \mu e) \lesssim \mathcal{O}(10^{-9})$ [48].

3.2.4 Measuring the Triple-Higgs Coupling

If the Englert-Brout-Higgs field gives masses to elementary particles, and if this field is itself elementary, and if the Higgs boson is the particle associated with this field, what gives a mass to the Higgs boson? The answer within the Standard Model is the Englert-Brout-Higgs field itself, via the triple-Higgs coupling. Examining the effective Lagrangian (35), we see the following terms:

$$\mathcal{L}_{\rm Higgs} \ni -\frac{\mu^2}{2}\eta^2 - \lambda v \eta^3 - \frac{1}{4}\eta^4 \,, \tag{94}$$

where η denotes the quantum fluctuation in the Englert-Brout-Higgs field around its classical v.e.v., see (29).

The triple-Higgs coupling may be measured via H pair production [69], which should be within reach of the LHC with high luminosity [8]. The dominant mechanism for HH production is expected to be gg fusion: $gg \to H^* \to HH$, with an important background from t and b box diagrams for $gg \to HH$. Another strategy for measuring the triple-Higgs coupling is indirectly via its effects on the cross section for $e^+e^- \to Z + H$ [70].

3.3 Supersymmetry

What else is there beyond the Higgs boson already discovered? Supersymmetry is my personal favourite candidate for physics beyond the Standard Model [5]. In my view, the discovery of a/the Higgs boson has strengthened the scientific case for supersymmetry. In addition to the traditional arguments that low-energy supersymmetry could resolve the fine-tuning (naturalness) aspect of the electroweak hierarchy problem, could provide the astrophysical dark matter, could facilitate grand unification and is essential (?) for string theory, we should remember that simple supersymmetric models stabilize the electroweak vacuum, predicted successfully the existence of a Higgs boson weighing < 130 GeV [71], and also predict (successfully, so far) that Higgs couplings should be within a few % of their Standard Model values. *No wonder I wrote the word 'supersymmetry' in the largest possible font on one of my slides!*

Historically, the first motivation for supersymmetry at the TeV scale came from considerations of quantum (loop) corrections to the Higgs mass-squared, m_H^2, and thereby to the electroweak scale [5]. For example, a generic fermionic loop such as that in Fig. 31(a) yields a correction:

$$\Delta m_H^2 = -\frac{y_f^2}{8\pi^2}[2\Lambda^2 + 6m_f^2 \ln(\Lambda/m_f) + ...], \tag{95}$$

where y_f is the Yukawa coupling: $y_f H\overline{\psi}\psi$, and Λ is an ultraviolet cutoff that represents the scale up to which the Standard Model remains valid, beyond which new physics appears. This contribution to the mass of the Higgs diverges quadratically with Λ. Hence if the Standard Model were to remain valid up to the Planck scale, $M_P \simeq 10^{19}$ GeV, so that $\Lambda = M_P$, this correction would be $\simeq 10^{34}$ times larger than the physical mass-squared of the Higgs, namely (10^2) GeV$)^2$. Moreover, the loop of a scalar field S, shown in Fig. 31(b), makes a similarly divergent contribution:

$$\Delta m_H^2 = \frac{\lambda_S}{16\pi^2}[\Lambda^2 - 2m_S^2 \ln(\Lambda/m_S) + ...], \tag{96}$$

where λ_S is the quartic coupling of S to the Higgs boson.

Comparing (95) and (96), we see that the quadratically-divergent terms $\propto \Lambda^2$ would cancel if, corresponding to every fermion f there is a scalar S with quartic coupling

$$\lambda_S \;=\; 2y_f^2 \,. \tag{97}$$

[8] Measuring the quadruple-Higgs coupling would require measuring triple-H production, which is likely to require a higher-energy collider such as the VHE-LHC described later.

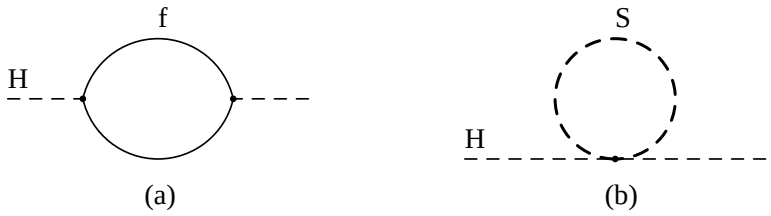

Fig. 31: One-loop quantum corrections to the mass-squared of the Higgs boson due to (a) the loop of a generic fermion f, (b) a generic scalar S.

This is exactly the relationship imposed by supersymmetry! Therefore, there are no quadratic divergences in supersymmetric field theories, not just at the one-loop level discussed above, but also at the multi-loop level [9]. This means that if there is some dynamical mechanism that imposes a large hierarchy between different physical mass scales at the tree level, supersymmetry anables it to be maintained in a natural way.

A different motivation for supersymmetry is provided by the measured mass of the Higgs boson. As already remarked, the electroweak vacuum would not be stable in the absence of any new physics, since the (negative) renormalization by top quark loops would drive the quartic Higgs self-coupling negative at some scale $\ll 10^{19}$ GeV, probably in the range 10^{10} to 10^{13} GeV. This could be averted if there were some new physics to counteract the negative renormalization by the top quark. In order to have the opposite sign to the top loop, this new physics should be bosonic, much like the stop squark [72] But then one must consider all the quartic bosonic couplings permitted (enforced) by renormalizability, end ensure that none of them blow up or generate an instability, which requires fine-tuning to one part in 10^3 in the simplest case studied. However, this fine-tuning could be made more natural by postulating a new fermion, much like the Higgsino. Thus, one finishes up with a theory that looks very much like supersymmetry!

Within a supersymmetric theory, the renormalization due to the top quark could prove to be a blessing in disguise! After cancelling the quadratic divergences in (95, 96), one is left with residual logarithmic divergences that can be resummed using the renormalization-group equations (RGEs). Not knowing how supersymmetry is broken, one often assumes that this occurs far above the TeV scale, e.g., around the grand unification or Planck scale, M_{GUT} or M_P. In this case, the Higgs and other supersymmetry-breaking masses for scalars and gauginos are renormalized significantly by time the electroweak scale is reached. At leading order in the RGEs, which resum the leading one-loop logarithms, the renormalizations of the soft gaugino masses M_a coincide with the corresponding gauge couplings:

$$Q\frac{dM_a}{dQ} \; = \; \beta_a M_a, \tag{98}$$

where β_a is the one-loop renormalization coefficient including supersymmetric particles. Hence, to leading order

$$M_a(Q) \; = \; \frac{\alpha_a(Q)}{\alpha_{GUT}} m_{1/2} \tag{99}$$

if the gaugino masses are assumed to have a universal value $m_{1/2}$ at the same large mass scale M_{GUT} as the gauge couplings α_a. For this reason, one expects the gluino to be heavier than the wino: $m_{\tilde{g}}/m_{\tilde{W}} \simeq \alpha_3/\alpha_2$ and the bino to be lighter again.

The gaugino masses contribute to the renormalizations of the soft supersymmetry-breaking scalar masses-squared m_i^2 via the gauge couplings, and the scalar masses and the trilinear soft supersymmetry

[9] Moreover, many logarithmic corrections to couplings are also cancelled in a supersymmetric theory.

breaking parameters A_λ contribute via the Yukawa couplings:

$$\frac{Qdm_i^2}{dQ} = \frac{1}{16\pi^2}\left[-g_a^2 M_a^2 + \lambda^2(m_i^2 + A_\lambda^2)\right]. \quad (100)$$

For most of the scalar partners of Standard Model fermions, one has at leading order

$$m_i^2(Q) = m_i^2 + C_i m_{1/2}^2, \quad (101)$$

where the coefficients C_i depends on the gauge quantum numbers of the corresponding fermion. Since renormalization by the strong coupling is largest, one expects the squarks to be heavier than the sleptons. Specifically, if all the m_i and the M_a are each assumed to be universal at the GUT scale (a scenario known as the CMSSM), at the electroweak scale one finds:

$$\text{Squarks}: \; m_{\tilde{q}}^2 \sim m_0^2 + 6m_{1/2}^2, \quad (102)$$

$$\text{Left}-\text{handed sleptons}: \; m_{\tilde{\ell}_L}^2 \sim m_0^2 + 0.5m_{1/2}^2, \quad (103)$$

$$\text{Right}-\text{handed sleptons}: \; m_{\tilde{\ell}_R}^2 \sim m_0^2 + 0.15m_{1/2}^2. \quad (104)$$

Typical results of calculations of these renormalization effects in the CMSSM are shown in Fig. 37.

Supersymmetry requires at least two Higgs doublets, one to give masses to charge-(+2/3) quarks, H_u, and the other to give masses to charge-(-1/3) quarks and charged leptons, H_d, and we denote the ratio of their v.e.v.s as $\tan\beta$. As we see in Fig. 32, renormalization by the top quark Yukawa coupling is important for one of the Higgs multiplets [10], and may drive $m_{H_u}^2$ negative at the electroweak scale. This may explain the negative sign of the quadratic term in the effective Standard Model potential, and would trigger electroweak symmetry breaking. If the top quark is heavy, it is possible for the electroweak scale to be generated naturally at a scale ~ 100 GeV if $m_t \sim 100$ GeV. For this reason, supersymmetry theorists actually suggested that the top quark should be heavy, before its discovery.

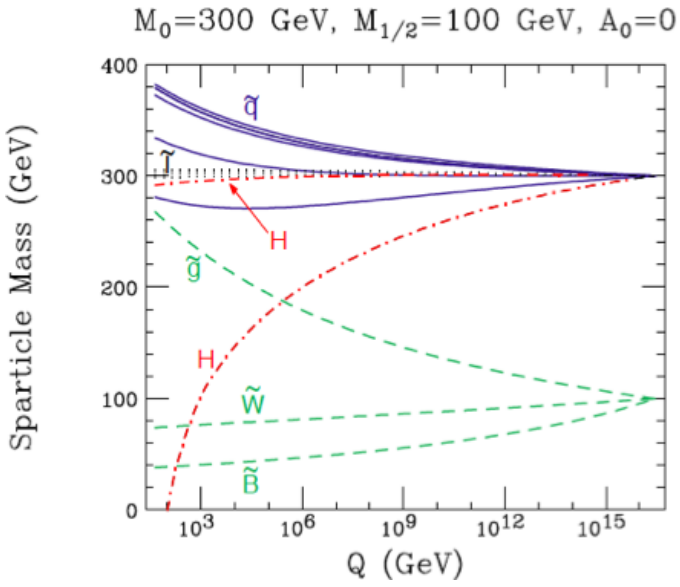

Fig. 32: Results of calculations of the renormalization of soft supersymmetry-breaking sparticle masses, assuming universal scalar and gaugino masses $m_0, m_{1/2}$ at M_{GUT}. In general, strongly-interacting sparticles have larger physical masses at low scales, and the $m_{H_u}^2$ is driven negative, triggering electroweak symmetry breaking.

[10] Renormalization by the other third-generation sfermions may also be important if $\tan\beta$ is large.

The two complex Higgs doublets of the MSSM have eight degrees of freedom, of which three are used by the Higgs mechanism for electroweak breaking to give masses to the $W^\pm$ bosons and to the Z^0, leaving five physical Higgs bosons in the physical spectrum. Of these, two (h, H) are neutral Higgs bosons that are CP-even (scalar), one (A) is neutral and CP-odd (pseudoscalar), and two are charged, the $H^\pm$. At tree level, the masses of the scalar supersymmetric Higgs bosons are:

$$m^2_{h,H} \; = \; \frac{1}{2}\left(m^2_A + m^2_Z \mp \sqrt{(m^2_A + m^2_Z)^2 - 4 m^2_A m^2_Z \cos^2 2\beta} \right) , \tag{105}$$

and the mass of the h is bounded from above by m_Z. This upper limit arises because the quartic Higgs coupling λ is fixed in the MSSM to be equal to the square of the electroweak gauge coupling (up to numerical factors), so that λ and hence m_{h^0} cannot be very large.

However, there are important radiative corrections to the above relations [71], the most important correction for m_h being the one-loop effect of the top quark and stop squark:

$$\Delta m^2_h = \frac{3 m^4_t}{4\pi^2 v^2} \ln\left(\frac{m_{\tilde{t}_1} m_{\tilde{t}_2}}{m^2_t} \right) + \ldots , \tag{106}$$

where $m_{\tilde{t}_{1,2}}$ are the physical masses of the stops. The correction Δm^2_h (106) depends quartically on the mass of the top, and after including this and higher-order corrections the mass of the lightest Higgs boson may be as large as [71, 73]:

$$m_h \lesssim 130 \text{ GeV}. \tag{107}$$

for stop masses of about a TeV, as seen in Fig. 33. The uncertainty in the calculation of m_h for given values of the supersymmetric model parameters is typically ~ 1.5 GeV. As noted earlier, the range (107) is perfectly consistent with the mass measured by ATLAS and CMS, yet another attractive feature of supersymmetry.

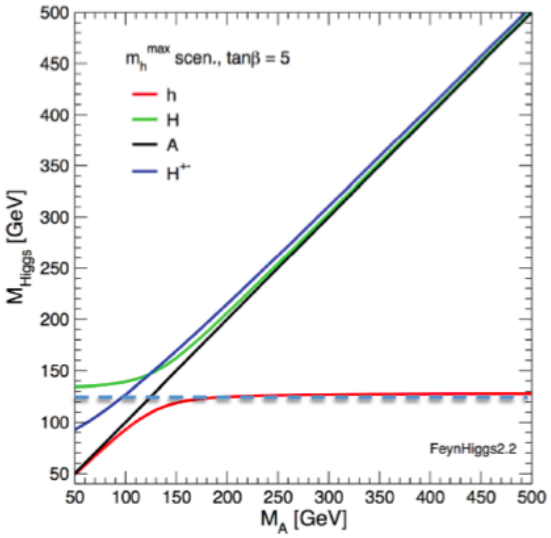

Fig. 33: The masses of the supersymmetric Higgs bosons as functions of m_A for fixed values of the other MSSM parameters.

In general, the couplings of the supersymmetric Higgs bosons differ from those in the Standard Model.

$$g_{hVV} \; = \; \sin(\beta - \alpha) g^{SM}_{HVV} , \tag{108}$$

$$g_{HVV} \; = \; \cos(\beta - \alpha) g^{SM}_{HVV} , \tag{109}$$

$$g_{hAZ} = \cos(\beta-\alpha)\frac{g'}{2\cos\theta_W}\,, \tag{110}$$

$$g_{h\bar{b}b}, g_{h\tau^+\tau^-} = -\frac{\sin\alpha}{\cos\beta} g^{SM}_{h\bar{b}b}\,, g^{SM}_{h\tau^+\tau^-}\,. \tag{111}$$

If $m_A \gg m_W$, the masses of the other four Higgs bosons are very similar: $m_H \sim m_A \sim m_{H^\pm}$. However, there is a different and interesting possibility of m_A is small, namely that $m_H \sim 125$ GeV, in which case the Higgs discovered at the LHC might actually be the second-lightest Higgs boson, and there might be a lighter one waiting to be discovered [74] [11]. Fig. 34 compares the predictions for various Higgs decays, relative to their Standard Model values, for fits in which the Higgs boson discovered is assumed to be the lightest one h (upper panel) and in which it is the heavier scalar H (lower panel). Overall, the quality of the conventional fit is better, but the unconventional fit may not yet be excluded. Experiments should continue the search for a lighter Higgs boson, remembering that it might have different couplings from those in the Standard Model.

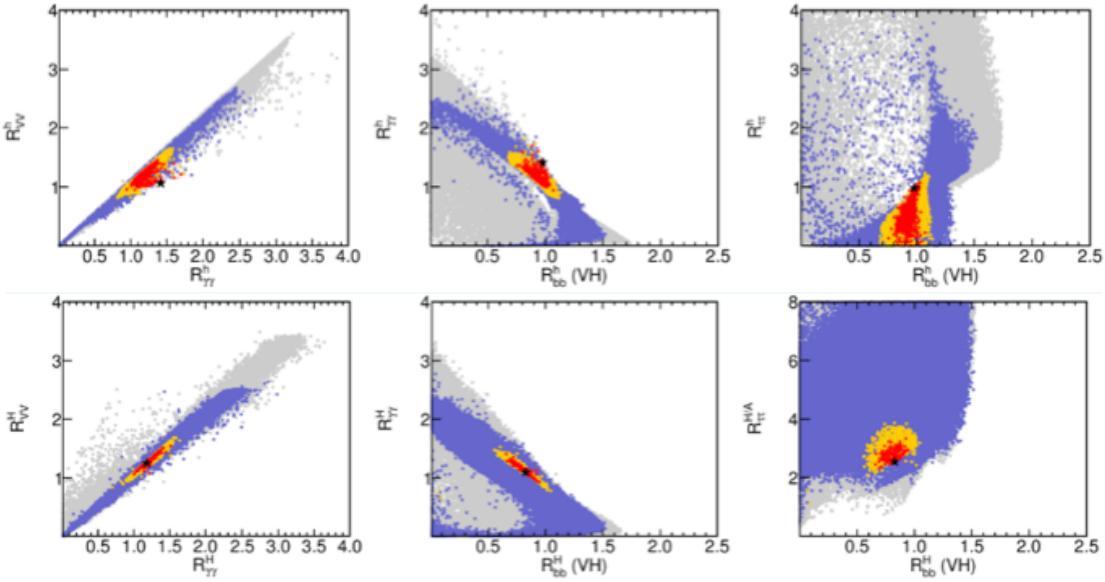

Fig. 34: Results of fits to Higgs data assuming (upper panel) that the Higgs boson discovered is the lightest supersymmetric Higgs h (upper panel) and in which it is the heavier scalar H (lower panel) [74].

3.4 Higgs and Supersymmetry

Let us now explore the implications for supersymmetry of the Higgs discovery, assuming that it is indeed the lighter scalar supersymmetric Higgs boson h. Important constraints on supersymmetric models are imposed by electroweak precision observables and flavour physics observables, the cosmological density [75] and astrophysical searches for cold dark matter [76], as well as LHC searches. In the following, we also take into account the experimental measurement of the anomalous magnetic moment of the muon, $g_\mu - 2$, which disagrees with theoretical calculations within the Standard Model by ~ 3 standard deviations [77]. This discrepancy could be explained by supersymmetry at a relatively low mass scale, although this possibility is disfavoured in simple supersymmetric models by the LHC Higgs mass measurement and the absence (so far) of direct evidence for supersymmetric particles at the LHC. Fig. 35 displays the relevant constraints provided by various ATLAS searches for supersymmetry with

[11] There are more possibilities for a lighter Higgs boson in the next-to-minimal supersymmetric extension of the Standard Model (NMSSM).

the full Run 1 data set of $\sim$ 20/fb of data at 8 TeV [78], using signatures with missing transverse energy (MET), jets, leptons and b quarks, interpreted within the CMSSM in which there are universal soft supersymmetry-breaking scalar masses m_0, gaugino masses $m_{1/2}$ and trilinear parameters $A_0 = -2m_0$ at the input GUT scale, assuming that $\tan\beta = 30$. We see that at small m_0 the most important constraint is provided by searches for jets + MET, whereas searches for leptons, b-jets and MET are more important at large m_0.

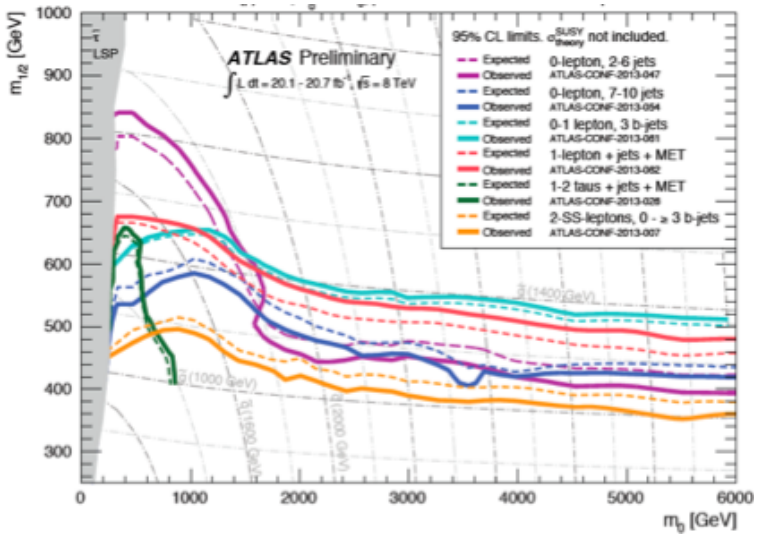

Fig. 35: Constraints on the universal soft supersymmetry-breaking scalar masses m_0, and gaugino masses $m_{1/2}$ of the CMSSM from ATLAS searches for supersymmetry with the full Run 1 data set of $\sim$ 20/fb of data at 8 TeV, using signatures with missing transverse energy (MET), jets, leptons and b quarks, assuming trilinear parameters $A_0 = -2m_0$ at the input GUT scale and $\tan\beta = 30$ [78].

In the following I present some results from a recent analysis [79] of these constraints made using the `MasterCode` framework [80], which incorporates a code for the electroweak observables based on [81], the flavour codes `SuFla` [82] and `SuperIso 3.3` [83], `SoftSUSY 3.3.9` [84] and `FeynHiggs 2.10.0` [73] for spectrum calculations, and the `MicrOMEGAs 3.2` [85] code for dark matter, which are interfaced using the SUSY Les Houches Accord [86]. We use the `MasterCode` framework to construct a global likelihood function (χ^2) that includes contributions from all the relevant observables.

Fig. 36 displays the regions of the $(m_0, m_{1/2})$ plane alowed at the 95% CL (blue lines) and favoured at the 68% CL (red lines) after taking all these constraints into account [79]. The solid lines and filled star are obtained using the current 20/fb ATLAS constraints, and the dashed lines and open star are based on the previous constraints from 7/fb of LHC data at 7 TeV. The m_h constraint has the effect of favouring relatively large values of $m_{1/2}$ beyond the reach of the direct LHC searches for supersymmetric particles, which have an impact only at low values of $m_{1/2}$. We note that the m_h constraint is relatively independent of m_0. Large values of $m_{1/2}$ are excluded by the dark matter density constraint.

The one-dimensional χ^2 function for the gluino mass $m_{\tilde{g}}$ resulting from this analysis of the CMSSM is shown in the upper left panel of Fig. 37 [79]. Again, the solid line is based on the current data set and the dotted line is based on the previous data set. We see that updating from the 7/fb 7-TeV data to the 20/fb 8-TeV data does not change the χ^2 function substantially. The current 95% CL lower limit on $m_{\tilde{g}} \sim 1350$ GeV. A similar plot for the mass of a generic supersymmetric partner of a right-handed quark is shown in the upper right panel of Fig. 37. In this case, the 95% CL lower limit is $m_{\tilde{q}_R} \sim 1650$ GeV. The lighter supersymmetric partner of the top quark may be significantly lighter, as shown in the lower left panel of Fig. 37, with a 95% CL lower limit $m_{\tilde{t}_1} \sim 750$ GeV. Finally, the corresponding plot for the lighter supersymmetric partner of the τ lepton is shown in the lower right

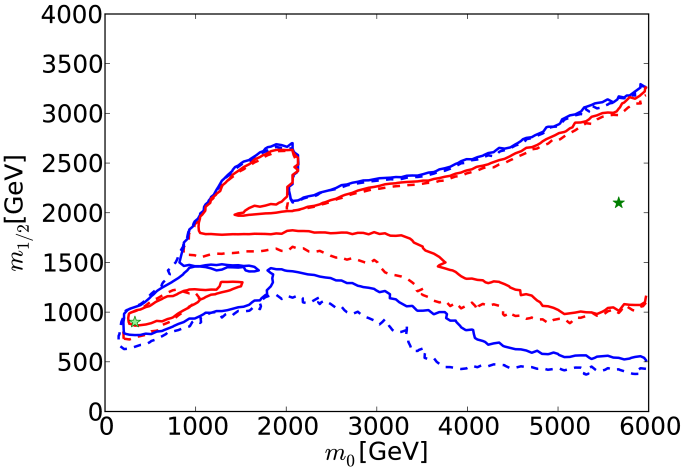

Fig. 36: The $(m_0, m_{1/2})$ plane in the CMSSM after implementing the constraints from ATLAS MET searches, precision electroweak.data, flavour physics, $g_\mu - 2$, m_h and dark matter. The results of the current CMSSM fit are indicated by solid lines and a filled star, and a fit to previous data is indicated by dashed lines and open stars. The red lines denote $\Delta\chi^2 = 2.30$ contours (corresponding approximately to the 68% CL), and the red lines denote $\Delta\chi^2 = 5.99$ (95% CL) contours [79].

panel of Fig. 37. This is expected to be the next-to-lightest supersymmetric particle, after the dark matter particle χ, and may have a mass as low as 330 GeV at the 95% CL.

Ref. [87] provides estimates of the supersymmetry discovery reach of the LHC with 14 TeV, e.g., the $(m_0, m_{1/2})$ plane displayed in Fig. 38. As seen there, the 5-σ discovery reach for squarks and gluinos with 300/fb of luminosity should be to $m_{\tilde{g}} \sim 3500$ GeV and $m_{\tilde{q}_R} \sim 2000$ GeV in the CMSSM, and the discovery range with 3000/fb of luminosity would extend a few hundred GeV further. Thus, large parts of the CMSSM parameter space will be accessible in future runs of the LHC [12]. The priorities and prospects for future colliders will depend whether the LHC discovers supersymmetry during its runs at 14 TeV, but certainly more detailed studies of the Higgs boson will be on the agenda of the LHC and future accelerators, as discussed in the last Section of these lectures.

3.5 What Accelerator Next: a Higgs Factory?

One of the possible options for a future accelerator is a 'Higgs Factory' designed to study the Higgs boson in detail. In fact, we already have a Higgs Factory, namely the LHC, which has already produced millions of Higgs bosons, though only a small fraction of them have been observed. High-energy runs of the LHC will start in 2015, and luminosity upgrades are being planned. Accordingly, the capabilities of the LHC are being rethought from the Higgs Factory perspective. However, although the upgraded LHC will produce orders of magnitude more Higgs bosons, its capabilities are limited by theoretical uncertainties in the production cross section as well as by the backgrounds that render unobservable some interesting decay modes.

Both these shortcomings would be avoided at a lepton collider, and various options are being considered. The most mature concept is a linear e^+e^- collider, and two projects are being developed: the ILC that would operate initially at energies up to 500 GeV [88], and CLIC that could possibly operate at energies up to 3 TeV [89], where the Higgs production cross section would be larger.

[12] It should be emphasized that the likelihood estimates made here are specific to the models studied, as are the estimates of the physics reaches.

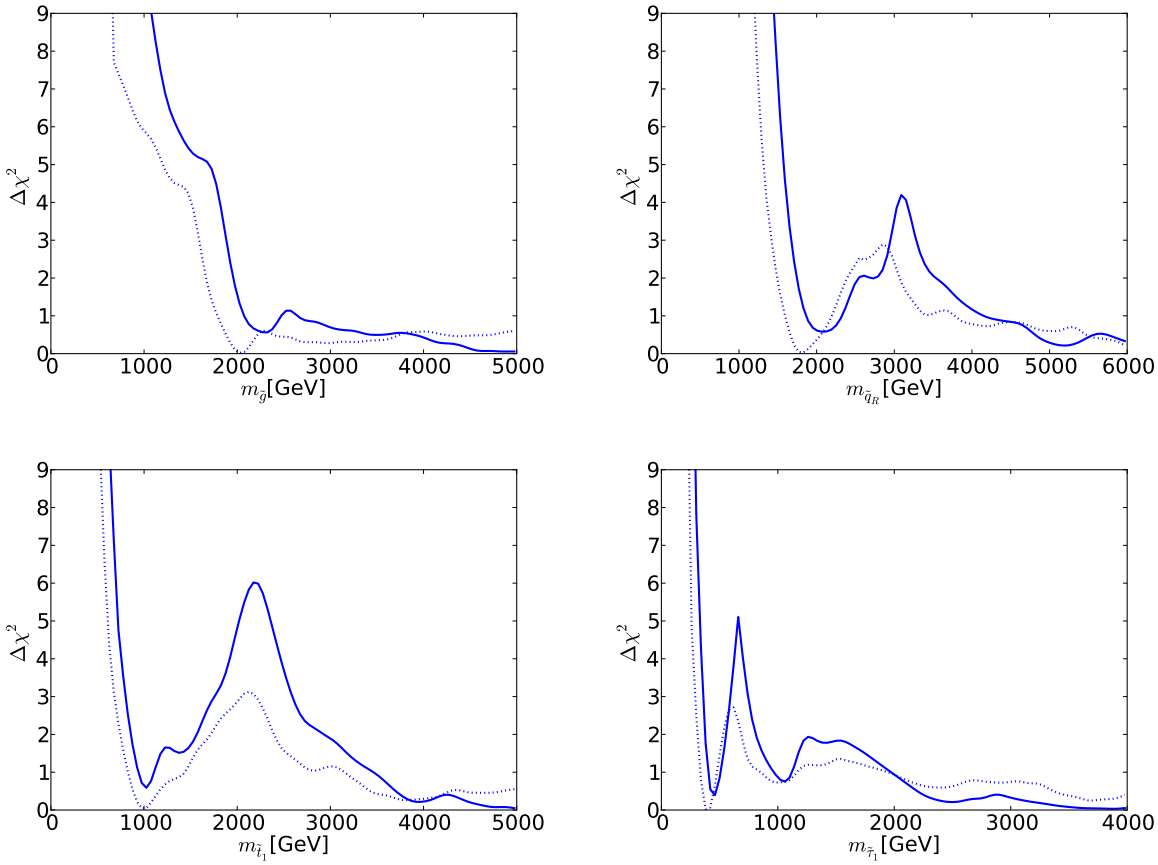

Fig. 37: The one-dimensional χ^2 likelihood functions in the CMSSM for $m_{\tilde{g}}$ (upper left), $m_{\tilde{q}_R}$ (upper right), $m_{\tilde{t}_1}$ (lower left) and $m_{\tilde{\tau}_1}$ (lower right). In each panel, the solid line is derived from a global analysis of the present data, and the dotted line is derived from an analysis of a previous data set, using current implementations of the constraints applied there [79].

In the last couple of years, the alternative possibility of a circular e^+e^- collider has been revived [90]. Proposals include LEP3, a design for a high-luminosity $\sqrt{s} = 240$ GeV e^+e^- collider that could be installed in the LHC tunnel, and TLEP, a $\sqrt{s} = 350$ to 500 GeV collider that could be installed in a larger tunnel with a circumference of 80 to 100 km. Also under consideration is a $\mu^+\mu^-$ collider, that would benefit from the (expected) larger coupling of the Higgs to the muon. Finally, there is the idea of a photon-photon collider, for example SAPPHiRE [91] that would exploit the recirculating linear accelerators proposed for the LHeC electron-proton collider.

Fig. 39 displays ATLAS estimates of the measurement uncertainties in Higgs signal strengths μ (left) and ratios of partial decay widths (right) with integrated luminosities of 300/fb (green) and 3000/fb (blue) [87] [13]. We see good prospects for significant improvements with 300/fb relative to the current measurements, and for further improvements with 3000/fb that would enable several Higgs couplings to be measured with accuracies $\lesssim 10$ %.

Fig. 40 displays estimates of the accuracies of measurements of the Higgs couplings to other particles that would be possible with the ILC [88], combining data from $\sqrt{s} = 250, 500$ and 1000 GeV. This figure exhibits the prospective improvements in testing the linear dependence of the couplings on the other particle masses expected in the Standard Model.

[13] The possible improvements in $\tau^+\tau^-$ measurements that could be provided by a more complete analysis are shown in brown.

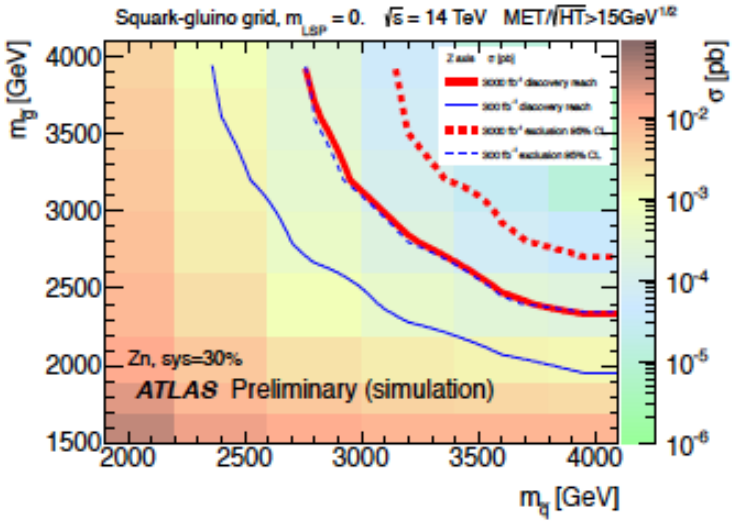

Fig. 38: The physics reach of the LHC in the $(m_0, m_{1/2})$ plane provided by searches for squarks and gluinos assuming that the LSP mass is negligible. the different colours represent the production cross section at 14 TeV. The solid (dashed) lines display the 5-σ discovery reach (95% CL exclusion limit) with 300/fb and 3000/fb respectively [87].

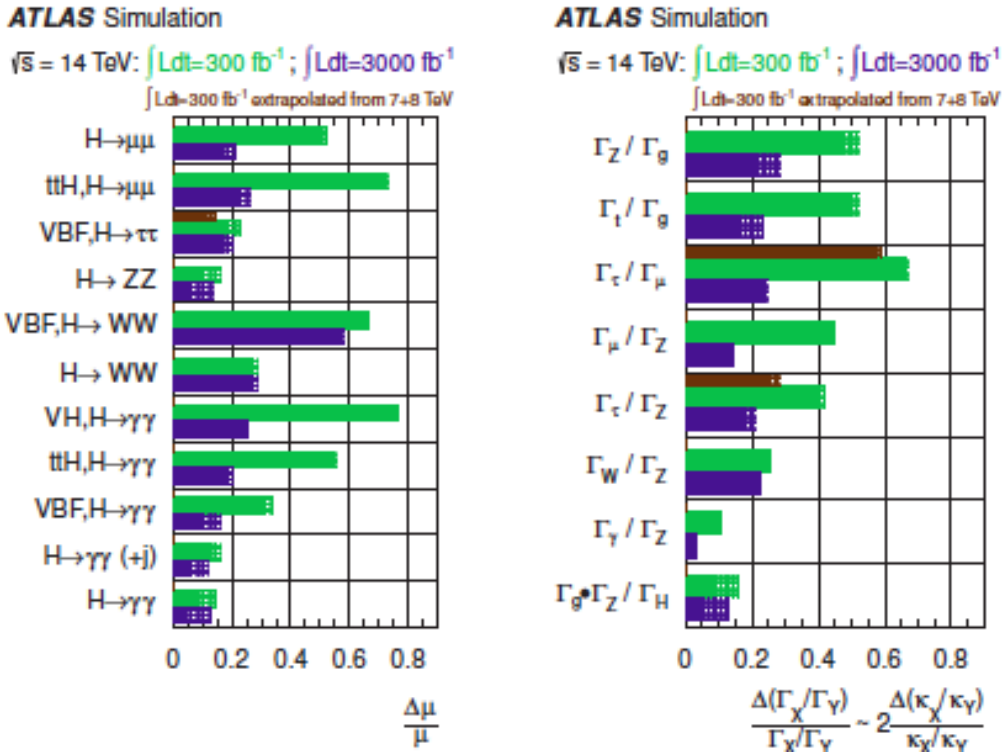

Fig. 39: Summary of ATLAS Higgs analysis sensitivities to signal strengths μ (left) and ratios of partial decay widths (right) with integrated luminosities of 300/fb (green) and 3000/fb at $\sqrt{s} = 14$ TeV for a Standard Model Higgs boson with a mass of 125 GeV [87].

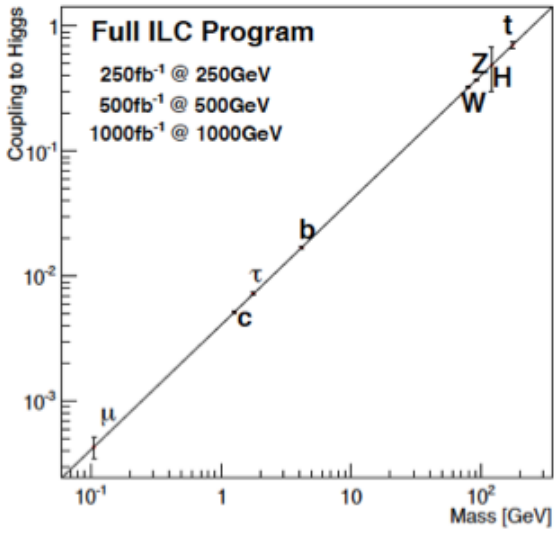

Fig. 40: Summary of the possible ILC accuracies for measurements of the Higgs couplings to other particles that could be obtained by combining data at 250, 500 and 1000 GeV [88].

As compared to linear e^+e^- colliders, circular colliders possess the feature that the achievable luminosity increases at lower energies, assuming that a fixed amount of power can be supplied to the beams. This feature is illustrated in Fig. 41 for the cases of TLEP, CLIC and the ILC [92]. Another feature of a circular e^+e^- collider is that it can accommodate multiple interaction points (IPs), whereas a linear collider has only a single IP, possibly with multiple detectors operated alternately in push-pull mode.

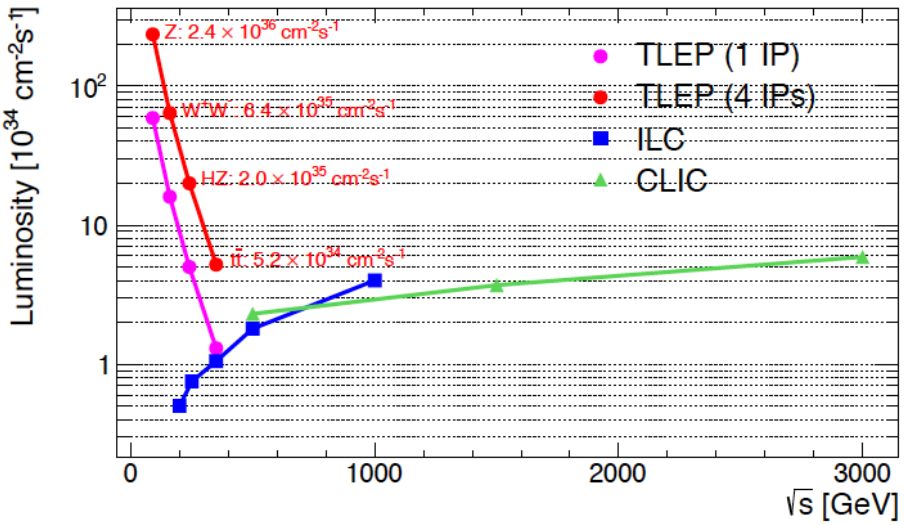

Fig. 41: Comparison of the luminosities estimated for TLEP with either one or four interaction points (IPs), CLIC and the ILC (which would have only a single IP) as functions of $\sqrt{s}$ [92].

The experimental conditions at circular and linear e^+e^- colliders are similar, with the difference that the bean energies are spread by beamstrahlung in the linear case and by synchrotron radiation in the circular case, which yields a lower probability of large energy loss. Preliminary studies of possible Higgs measurements at TLEP have been made with simulations of the CMS detector that was designed for LHC physics [92]. Fig. 42 shows one example, that of the process $e^+e^- \to H + Z$ followed by

$H \to e^+e^-, \mu^+\mu^-$: a detector specifically designed for e^+e^- collisions such as those developed for the ILC or CLIC would undoubtedly improve on these measurements.

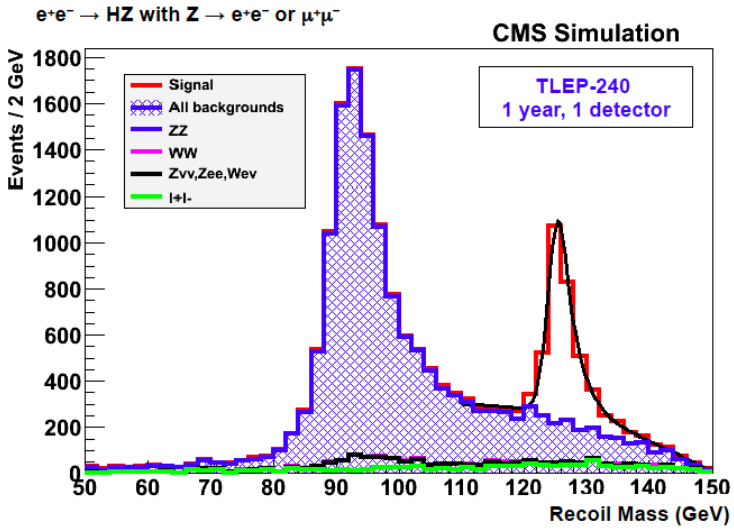

Fig. 42: Example of a simulation of the process $e^+e^- \to H + Z$ followed by $H \to e^+e^-, \mu^+\mu^-$ at TLEP using a simulation of the CMS detector that was designed for LHC physics [92].

Fig. 43 shows a comparison of the estimated uncertainties in possible measurements of Higgs couplings with the high-luminosity upgrade of the LHC at $\sqrt{s} = 14$ TeV (HL-LHC, green), the ILC (blue) and TLEP (red) operating at $\sqrt{s} = 350$ GeV [92]. In the case of the HL-LHC, just one experiment is included, and the dashed lines neglect the possibility of improved theoretical calculations leading to reduced theoretical uncertainties. In each case, we see that TLEP could provide an accuracy considerably superior to that of the ILC, which is traceable directly to the higher statistics made available by the higher luminosity of TLEP visible in Fig. 41.

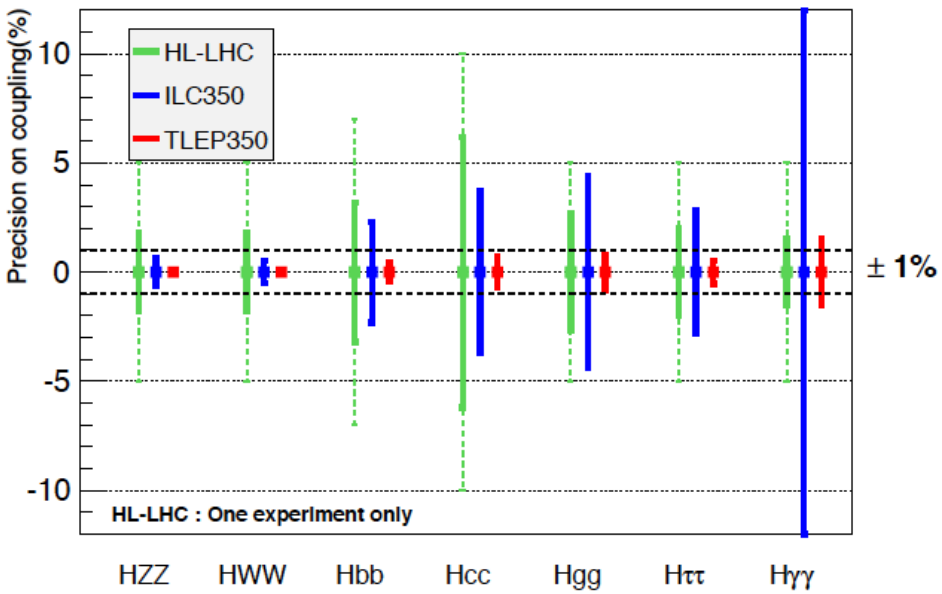

Fig. 43: Comparison of the estimated uncertainties of measurements of Higgs couplings with the high-luminosity upgrade of the LHC (HL-LHC, green), the ILC (blue) and TLEP (red) operating at $\sqrt{s} = 350$ GeV [92].

Fig. 44 shows the result of a two-parameter (M, ϵ) fit (83) to the TLEP coupling measurements listed in Figs. 43, assuming the same central values as the Standard Model, which yields

$$M \; = \; 246.0 \pm 0.8 \; \mathrm{GeV}, \; \epsilon \; = \; 0.0000^{+0.0015}_{-0.0010} \, , \tag{112}$$

offering the possibility of probing the Standard Model couplings at the few per-mille level. From this analysis we see that TLEP offers peerless capabilities for measuring Higgs properties. It is worth mentioning that TLEP also offers unique possibilities for other precision measurements of the Standard Model, e.g., at the Z^0 peak and in W^+W^- production. However, the full exploitation of these accurate measurements will require a new generation of high-precision calculations within the Standard Model, posing a challenge to the theoretical community.

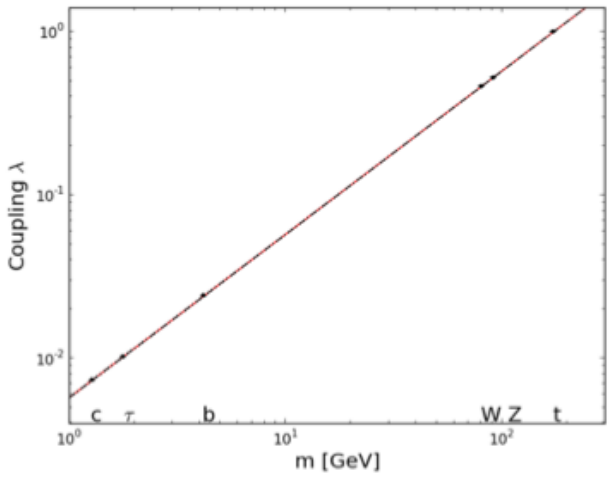

Fig. 44: The result of a two-parameter (M, ϵ) fit (83) to the TLEP coupling measurements listed in Figs. 43, assuming the same central values as the Standard Model, to be compared with the left panel of Fig. 21.

This point is exemplified in Fig. 45. The horizontal bars represent the experimental accuracies with which various Higgs couplings can be measured at the LHC with 300/fb of luminosity, at the HL-LHC with 3000/fb of luminosity, at the ILC and at TLEP. Also shown are the deviations from the Standard Model predictions for various Higgs branching ratios calculated in typical supersymmetric fits within the models described in the previous Section. The good news is that TLEP would have sufficient precision to distinguish these models from the Standard Model. Unfortunately, there is some bad news as well. Fig. 45 that shows the current theoretical uncertainties in these branching ratios quoted by the LHC Higgs cross-section working group [39] dwarf the TLEP experimental uncertainties. More precise theoretical calculations will be sorely needed.

3.6 A Vision for the Future

It would be premature to decide on the top priority for a possible future large collider before we see at least some first results from the LHC at 13/14 TeV. The physics landscape will be completely different if supersymmetric particles or some other new physics is discovered at the TeV scale. In my opinion, in that case it would be a mistake to invest the world's particle physics resources in a collider incapable of studying the new TeV-scale physics.

Beyond any reasonable doubt, the ATLAS and CMS experiments at the LHC have discovered a Higgs boson, but it remains an open question whether there may be others. However, the existence of an (apparently) elementary scalar boson poses a big challenge for theoretical physics. Most of the responses to this challenge postulate some new physics at the TeV scale. There is some puzzlement that no such

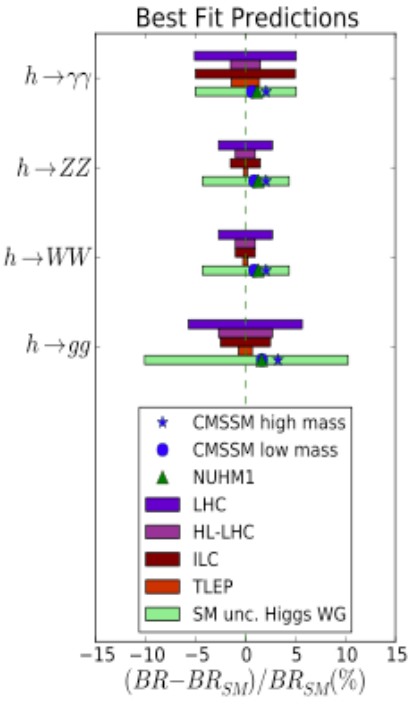

Fig. 45: From top to bottom: uncertainties in the measurements of Higgs branching ratios that may be made at the LHC with 300/fb, the HL-LHC with 3000/fb, the ILC and TLEP, and finally the current theoretical uncertainties within the Standard Model. Also shown are the deviations from Standard Model predictions found in representative fits within supersymmetric models [92].

new physics turned up in the first LHC run at 7 and 8 TeV, but it is too soon for disappointment, still less despair. The LHC has broad possibilities for discovering new physics beyond the Standard Model when it restarts at 13/14 TeV. If it does discover new physics at the TeV scale, the top priority will be to study it, and beyond the LHC, a very-high-energy pp collider may offer the best prospects for long-term studies of this new physics. If the LHC does not discover more new physics, it would be natural to focus on studies of the Higgs boson that has already been discovered, in which case TLEP offers the best prospects, also for other high-precision physics.

The TLEP project is part of a vision for the future of particle physics that combines indirect exploration of possible new physics at the 10-TeV scale in e^+e^- collisions with direct exploration of this energy scale in very-high-energy pp collisions at $\sqrt{s} \lesssim 100$ TeV in the same tunnel with a circumference of 80 to 100 km [93]. The communities interested in these complementary exploratory projects should work together to realize this vision, whose physics case will require a major effort to develop and convince those who control the global resources for scientific research.

Acknowledgements

I thank Tevong You for his collaboration on topics discussed in these lectures. I also thank fellow members of the MasterCode Collaboration, particularly Oliver Buchmueller, Sven Heinemeyer, Jad Marrouche, Keith Olive and Kees de Vries for many discussions. I also thank members of the TLEP Study Group, including Alain Blondel, Patrick Janot, Mike Koratzinos and Frank Zimmermann for many discussions. This work was supported in part by the London Centre for Terauniverse Studies (LCTS), using funding from the European Research Council via the Advanced Investigator Grant 267352.

References

[1] G. Aad *et al.* [ATLAS Collaboration], Phys. Lett. B **716** (2012) 1 [arXiv:1207.7214 [hep-ex]].

[2] S. Chatrchyan *et al.* [CMS Collaboration], Phys. Lett. B **716** (2012) 30 [arXiv:1207.7235 [hep-ex]].

[3] S. Weinberg, Phys. Rev. Lett. **19**, 1264 (1967).

[4] A. Salam, in the *Proceedings of 8th Nobel Symposium*, Lerum, Sweden, 19-25 May 1968, pp 367-377.

[5] M. Bustamante, L. Cieri and J. Ellis, CERN Yellow Report CERN-2010-001, 145-228 [arXiv:0911.4409 [hep-ph]].

[6] E. Boos, Lectures at this School.

[7] S. L. Glashow, Nucl. Phys. **22** (1961) 579.

[8] LEP Electroweak Working Group, `http://lepewwg.web.cern.ch/LEPEWWG/`.

[9] Gftitter Group `http://project-gfitter.web.cern.ch/project-gfitter/`.

[10] J. Bardeen, L. N. Cooper and J. R. Schrieffer, Phys. Rev. **106** (1957) 162; V. L. Ginzburg and L. D. Landau, Zh. Eksp. Teor. Fiz. **20** (1950) 1064 and Phys. Rev. **108** (1957) 1175; L. N. Cooper, Phys. Rev. **104** (1956) 1189.

[11] Y. Nambu, Phys. Rev. Lett. **4** (1960) 380.

[12] J. Goldstone, Nuovo Cim. **19** (1961) 154;

[13] J. Goldstone, A. Salam and S. Weinberg, Phys. Rev. **127** (1962) 965.

[14] Y. Nambu, Phys. Rev. **117** (1960) 648.

[15] P. W. Anderson, Phys. Rev. **130** (1963) 439;

[16] W. Gilbert, Phys. Rev. Lett. **12** (1964) 713.

[17] F. Englert and R. Brout, Phys. Rev. Lett. **13** (1964) 321.

[18] P. W. Higgs, Phys. Lett. **12** (1964) 132.

[19] P. W. Higgs, Phys. Rev. Lett. **13** (1964) 508.

[20] G. S. Guralnik, C. R. Hagen and T. W. B. Kibble, Phys. Rev. Lett. **13** (1964) 585.

[21] A. A. Migdal and A. M. Polyakov, Sov. Phys. JETP **24** (1967) 91 [Zh. Eksp. Teor. Fiz. **51** (1966) 135].

[22] T. W. B. Kibble, Phys. Rev. **155** (1967) 1554.

[23] P. W. Higgs, Phys. Rev. **145** (1966) 1156.

[24] For some pre-LHC review of electroweak theory, see C. Quigg, Ann. Rev. Nucl. Part. Sci. **59** (2009) 505 [arXiv:0905.3187 [hep-ph]]; M. Bustamante, L. Cieri and J. Ellis, CERN Yellow Report CERN-2010-001, 145-228 [arXiv:0911.4409 [hep-ph]].

[25] G. 't Hooft, Nucl. Phys. B **33** (1971) 173 and Nucl. Phys. B **35** (1971) 167; G. 't Hooft and M. J. G. Veltman, Nucl. Phys. B **44** (1972) 189.

[26] J. M. Cornwall, D. N. Levin and G. Tiktopoulos, Phys. Rev. Lett. **30** (1973) 1268 [Erratum-ibid. **31** (1973) 572].

[27] C. H. Llewellyn Smith, Phys. Lett. B **46** (1973) 233.

[28] J. S. Bell, Nucl. Phys. B **60** (1973) 427.

[29] J. R. Ellis, M. K. Gaillard and D. V. Nanopoulos, Nucl. Phys. B **106** (1976) 292.

[30] J. Ellis and M. K. Gaillard, *Theoretical remarks*, in L. Camilleri *et al.*, *Physics with very high-energy e^+e^- colliding beams*, CERN report 76-18 (Nov. 1976), pp 21-94.

[31] LEP Higgs Working Group, `http://lephiggs.web.cern.ch/LEPHIGGS/www/Welcome.html`.

[32] R. Barate *et al.* [LEP Working Group for Higgs boson searches and ALEPH, DELPHI, L3 and OPAL Collaborations], Phys. Lett. B **565** (2003) 61 [hep-ex/0306033].

[33] Tevatron New Phenomena and Higgs Working Group, `http://tevnphwg.fnal.gov/`.

[34] M. J. G. Veltman, Nucl. Phys. B **123** (1977) 89.

[35] M. J. G. Veltman, Acta Phys. Polon. B **8** (1977) 475.

[36] J. R. Ellis and G. L. Fogli, Phys. Lett. B **249** (1990) 543, J. R. Ellis, G. L. Fogli and E. Lisi, Phys. Lett. B **274** (1992) 456 and Phys. Lett. B **318** (1993) 148.

[37] M. Baak, M. Goebel, J. Haller, A. Hoecker, D. Ludwig, K. Moenig, M. Schott and J. Stelzer, Eur. Phys. J. C **72** (2012) 2003 [arXiv:1107.0975 [hep-ph]].

[38] H. M. Georgi, S. L. Glashow, M. E. Machacek and D. V. Nanopoulos, Phys. Rev. Lett. **40** (1978) 692.

[39] S. Dittmaier *et al.* [LHC Higgs Cross Section Working Group Collaboration], arXiv:1101.0593 [hep-ph]; arXiv:1201.3084 [hep-ph].

[40] R. N. Cahn and S. Dawson, Phys. Lett. B **136** (1984) 196 [Erratum-ibid. B **138** (1984) 464].

[41] S. L. Glashow, D. V. Nanopoulos and A. Yildiz, Phys. Rev. D **18** (1978) 1724.

[42] F. Maltoni, K. Paul, T. Stelzer and S. Willenbrock, Phys. Rev. D **64** (2001) 094023 [hep-ph/0106293].

[43] S. Biswas, E. Gabrielli and B. Mele, JHEP **1301** (2013) 088 [arXiv:1211.0499 [hep-ph]]; S. Biswas, E. Gabrielli, F. Margaroli and B. Mele, JHEP **07** (2013) 073 [arXiv:1304.1822 [hep-ph]].

[44] J. Ellis, D. S. Hwang, K. Sakurai and M. Takeuchi, KCL-PH-TH/2013-47, LCTS/2013-35, CERN-PH-TH/2013-312.

[45] S. Heinemeyer *et al.* [LHC Higgs Cross Section Working Group Collaboration], arXiv:1307.1347 [hep-ph].

[46] ATLAS Collaboration, `https://cds.cern.ch/record/1632191/files/ATLAS-CONF-2013-108.p`
CMS Collaboration, `https://twiki.cern.ch/twiki/bin/view/CMSPublic/Hig13004TWikiUpd`

[47] ATLAS Collaboration, `https://twiki.cern.ch/twiki/bin/view/AtlasPublic/HiggsPublicR`
CMS Collaboration, `https://twiki.cern.ch/twiki/bin/view/CMSPublic/PhysicsResultsHI`

[48] G. Blankenburg, J. Ellis and G. Isidori, Phys. Lett. B **712** (2012) 386 [arXiv:1202.5704 [hep-ph]]; R. Harnik, J. Kopp and J. Zupan, JHEP **1303** (2013) 026 [arXiv:1209.1397 [hep-ph]].

[49] G. Degrassi, S. Di Vita, J. Elias-Miro, J. R. Espinosa, G. F. Giudice, G. Isidori and A. Strumia, JHEP **1208** (2012) 098 [arXiv:1205.6497 [hep-ph]].

[50] A. Juste, S. Mantry, A. Mitov, A. Penin, P. Skands, E. Varnes, M. Vos and S. Wimpenny, arXiv:1310.0799 [hep-ph].

[51] J. Ellis and T. You, JHEP **1306** (2013) 103 [arXiv:1303.3879 [hep-ph]].

[52] J. Ellis, D. S. Hwang, V. Sanz and T. You, JHEP **1211** (2012) 134 [arXiv:1208.6002 [hep-ph]];

[53] D0 Collaboration, `http://www-d0.fnal.gov/Run2Physics/WWW/results/prelim/HIGGS/H138/` and `http://www-d0.fnal.gov/Run2Physics/WWW/results/prelim/HIGGS/H139/`.

[54] J. Ellis, V. Sanz and T. You, Eur. Phys. J. C **73** (2013) 2507 [arXiv:1303.0208 [hep-ph]];

[55] See, for example: J. Ellis and D. S. Hwang, JHEP **1209** (2012) 071 [arXiv:1202.6660 [hep-ph]];

[56] J. Ellis, R. Fok, D. S. Hwang, V. Sanz and T. You, Eur. Phys. J. C **73** (2013) 2488 [arXiv:1210.5229 [hep-ph]].

[57] S. Bolognesi, Y. Gao, A. V. Gritsan, K. Melnikov, M. Schulze, N. V. Tran and A. Whitbeck, Phys. Rev. D **86** (2012) 095031 [arXiv:1208.4018 [hep-ph]].

[58] J. Ellis, V. Sanz and T. You, Phys. Lett. B **726** (2013) 244 [arXiv:1211.3068 [hep-ph]].

[59] G. Aad *et al.* [ATLAS Collaboration], Phys. Lett. B **726** (2013) 120 [arXiv:1307.1432 [hep-ex]].

[60] Here the analysis in [51] is used. For a partial list of previous references, see: D. Carmi, A. Falkowski, E. Kuflik and T. Volanski, arXiv:1202.3144 [hep-ph]; A. Azatov, R. Contino and J. Galloway, JHEP **1204** (2012) 127 [hep-ph/1202.3415]. J.R. Espinosa, C. Grojean, M. Muhlleitner and M. Trott, arXiv:1202.3697 [hep-ph]; P. P. Giardino, K. Kannike, M. Raidal and

A. Strumia, arXiv:1203.4254 [hep-ph]; T. Li, X. Wan, Y. Wang and S. Zhu, arXiv:1203.5083 [hep-ph]; M. Rauch, arXiv:1203.6826 [hep-ph]; J. Ellis and T. You, JHEP **1206** (2012) 140, [arXiv:1204.0464 [hep-ph]]; A. Azatov, R. Contino, D. Del Re, J. Galloway, M. Grassi and S. Rahatlou, arXiv:1204.4817 [hep-ph]; M. Klute, R. Lafaye, T. Plehn, M. Rauch and D. Zerwas, arXiv:1205.2699 [hep-ph]; L. Wang and X.-F. Han, Phys. Rev. D **86** (2012) 095007, [arXiv:1206.1673 [hep-ph]]; D. Carmi, A. Falkowski, E. Kuflik and T. Volansky, arXiv:1206.4201 [hep-ph]; M. J. Dolan, C. Englert and M. Spannowsky, arXiv:1206.5001 [hep-ph]; J. Chang, K. Cheung, P. Tseng and T. Yuan, arXiv:1206.5853 [hep-ph]; S. Chang, C. A. Newby, N. Raj and C. Wanotayaroj, arXiv:1207.0493 [hep-ph]; I. Low, J. Lykken and G. Shaughnessy, arXiv:1207.1093 [hep-ph]; T. Corbett, O. J. P. Eboli, J. Gonzalez-Fraile and M. C. Gonzalez-Garcia, arXiv:1207.1344 [hep-ph]; P. P. Giardino, K. Kannike, M. Raidal and A. Strumia, arXiv:1207.1347 [hep-ph]; M. Montull and F. Riva, arXiv:1207.1716 [hep-ph]; J. R. Espinosa, C. Grojean, M. Muhlleitner and M. Trott, arXiv:1207.1717 [hep-ph]; D. Carmi, A. Falkowski, E. Kuflik, T. Volansky and J. Zupan, arXiv:1207.1718 [hep-ph]; S. Banerjee, S. Mukhopadhyay and B. Mukhopadhyaya, JHEP **10** (2012) 062, [arXiv:1207.3588 [hep-ph]]; F. Bonner, T. Ota, M. Rauch and W. Winter, arXiv:1207.4599 [hep-ph]; T. Plehn and M. Rauch, arXiv:1207.6108 [hep-ph]; A. Djouadi, arXiv:1208.3436 [hep-ph]; B. Batell, S. Gori and L. T. Wang, arXiv:1209.6832 [hep-ph]; G. Moreau, Phys. Rev. D **87** (2013) 015027, [arXiv:1210.3977 [hep-ph]]; G. Cacciapaglia, A. Deandrea, G. D. La Rochelle and J-B. Flament, arXiv:1210.8120 [hep-ph]; E. Masso and V. Sanz, arXiv:1211.1320 [hep-ph]; T. Corbett, O. J. P. Ebol, J. Gonzalez-Fraile and M. C. Gonzalez-Garcia, arXiv:1211.4580 [hep-ph]; R. Tito D'Agnolo, E. Kuflik and M. Zanetti, arXiv:1212.1165 [hep-ph]; A. Azatov and J. Galloway, arXiv:1212.1380 [hep-ph]; G. Bhattacharyya, D. Das and P.B. Pal, Phys. Rev. D **87** (2013) 011702, [arXiv:1212.4651 [hep-ph]]; D. Choudhury, R. Islam, A. Kundu and B. Mukhopadhyaya, arXiv:1212.4652 [hep-ph]; R. S. Gupta, M. Montull and F. Riva, arXiv:1212.5240 [hep-ph]; G. Belanger, B. Dumont, U. Ellwanger, J. F. Gunion and S. Kraml, arxiv:1212.5244 [hep-ph]; K. Cheung, J. S. Lee and P-Y. Tseng, arXiv:1302.3794 [hep-ph].

[61] J. Ellis and T. You, JHEP **1209** (2012) 123 [arXiv:1207.1693 [hep-ph]].

[62] F. Caola and K. Melnikov, Phys. Rev. D **88** (2013) 054024 [arXiv:1307.4935 [hep-ph]].

[63] J. M. Campbell, R. K. Ellis and C. Williams, arXiv:1311.3589 [hep-ph].

[64] J. M. Campbell, R. K. Ellis and C. Williams, arXiv:1312.1628 [hep-ph].

[65] L. J. Dixon and Y. Li, Phys. Rev. Lett. **111** (2013) 111802 [arXiv:1305.3854 [hep-ph]].

[66] Class for Physics of the Royal Swedish Academy of Sciences, `http://www.nobelprize.org/nobel_prizes/physics/laureates/2013/advanced-physicsprize2013.pdf`.

[67] S. Weinberg, Rev. Mod. Phys. **61** (1989) 1.

[68] For an introduction to the extensive literature, see A. Alloul, B. Fuks and V. Sanz, arXiv:1310.5150 [hep-ph]; C. Y. Chen, S. Dawson and C. Zhang, arXiv:1311.3107 [hep-ph].

[69] See, for example M. J. Dolan, C. Englert and M. Spannowsky, JHEP **1210** (2012) 112 [arXiv:1206.5001 [hep-ph]].

[70] M. McCullough, arXiv:1312.3322 [hep-ph].

[71] Y. Okada, M. Yamaguchi and T. Yanagida, Prog. Theor. Phys. **85** (1991) 1; J. R. Ellis, G. Ridolfi and F. Zwirner, Phys. Lett. B **257** (1991) 83; H. E. Haber and R. Hempfling, Phys. Rev. Lett. **66** (1991) 1815.

[72] J. R. Ellis and D. Ross, Phys. Lett. B **506** (2001) 331 [hep-ph/0012067].

[73] For the most recent calculations of supersymmetric Higgs masses, including leading and next-to-leading contributions beyond two loops, see: T. Hahn, S. Heinemeyer, W. Hollik, H. Rzehak and G. Weiglein, arXiv:1312.4937 [hep-ph].

[74] P. Bechtle, S. Heinemeyer, O. Stal, T. Stefaniak, G. Weiglein and L. Zeune, Eur. Phys. J. C **73**

(2013) 2354 [arXiv:1211.1955 [hep-ph]].

[75] J. R. Ellis, J. S. Hagelin, D. V. Nanopoulos, K. A. Olive and M. Srednicki, Nucl. Phys. B **238** (1984) 453; H. Goldberg, Phys. Rev. Lett. **50** (1983) 1419 [Erratum-ibid. **103** (2009) 099905].

[76] D. S. Akerib *et al.* [LUX Collaboration], arXiv:1310.8214 [astro-ph.CO].

[77] G. Bennett et al. [The Muon g-2 Collaboration], Phys. Rev. D **73** (2006) 072003 [arXiv:hep-ex/0602035]; M. Benayoun, P. David, L. DelBuono and F. Jegerlehner, Eur. Phys. J. C **73** (2013) 2453 [arXiv:1210.7184 [hep-ph]]; T. Blum, A. Denig, I. Logashenko, E. de Rafael, B. L. Roberts, T. Teubner and G. Venanzoni, arXiv:1311.2198 [hep-ph].

[78] ATLAS Collaboration, `http://cds.cern.ch/record/1547563/ files/ATLAS-CONF-2013-047.pdf`.

[79] O. Buchmueller, R. Cavanaugh, A. De Roeck, M. J. Dolan, J. R. Ellis, H. Flacher, S. Heinemeyer and G. Isidori *et al.*, arXiv:1312.5250 [hep-ph], see also O. Buchmueller, M. J. Dolan, J. Ellis, T. Hahn, S. Heinemeyer, W. Hollik, J. Marrouche and K. A. Olive *et al.*, arXiv:1312.5233 [hep-ph].

[80] MasterCode Collaboration, `http://mastercode.web.cern.ch/mastercode/`.

[81] S. Heinemeyer *et al.*, JHEP **0608** (2006) 052 [arXiv:hep-ph/0604147]; S. Heinemeyer, W. Hollik, A. M. Weber and G. Weiglein, JHEP **0804** (2008) 039 [arXiv:0710.2972 [hep-ph]].

[82] G. Isidori and P. Paradisi, Phys. Lett. B **639** (2006) 499 [arXiv:hep-ph/0605012]; G. Isidori, F. Mescia, P. Paradisi and D. Temes, Phys. Rev. D **75** (2007) 115019 [arXiv:hep-ph/0703035], and references therein.

[83] F. Mahmoudi, Comput. Phys. Commun. **178** (2008) 745 [arXiv:0710.2067 [hep-ph]]; Comput. Phys. Commun. **180** (2009) 1579 [arXiv:0808.3144 [hep-ph]]; D. Eriksson, F. Mahmoudi and O. Stal, JHEP **0811** (2008) 035 [arXiv:0808.3551 [hep-ph]].

[84] B. C. Allanach, Comput. Phys. Commun. **143** (2002) 305 [arXiv:hep-ph/0104145].

[85] G. Belanger, F. Boudjema, A. Pukhov and A. Semenov, Comput. Phys. Commun. **176** (2007) 367 [arXiv:hep-ph/0607059]; Comput. Phys. Commun. **149** (2002) 103 [arXiv:hep-ph/0112278]; Comput. Phys. Commun. **174** (2006) 577 [arXiv:hep-ph/0405253].

[86] P. Skands *et al.*, JHEP **0407** (2004) 036 [arXiv:hep-ph/0311123]; B. Allanach *et al.*, Comput. Phys. Commun. **180** (2009) 8 [arXiv:0801.0045 [hep-ph]].

[87] ATLAS Collaboration, arXiv:1307.7292 [hep-ex].

[88] ILC TDR, H. Baer, T. Barklow, K. Fujii, Y. Gao, A. Hoang, S. Kanemura, J. List and H. E. Logan *et al.*, arXiv:1306.6352 [hep-ph].

[89] CLIC CDR, eds. M. Aicheler, P. Burrows, M. Draper, T. Garvey, P. Lebrun, K. Peach, N. Phinney, H. Schmickler, D. Schulte and N. Toge, CERN-2012-007, `http://project-clic-cdr.web.cern.ch/project-CLIC-CDR/`.

[90] A. Blondel and F. Zimmermann, arXiv:1112.2518; A. Blondel, M. Koratzinos, R. W. Assmann, A. Butterworth, P. Janot, J. M. Jimenez, C. Grojean and A. Milanese *et al.*, arXiv:1208.0504 [physics.acc-ph].

[91] S. A. Bogacz, J. Ellis, L. Lusito, D. Schulte, T. Takahashi, M. Velasco, M. Zanetti and F. Zimmermann, arXiv:1208.2827 [physics.acc-ph].

[92] M. Bicer, H. Duran Yildiz, I. Yildiz, G. Coignet, M. Delmastro, T. Alexopoulos, C. Grojean and S. Antusch *et al.*, arXiv:1308.6176 [hep-ex].

[93] Future Circular Collider Study, `http://indico.cern.ch/conferenceDisplay.py?confId=28234`